Decomposed Linear Dynamical Systems (dLDS) models reveal context-dependent dynamic connectivity in *C. elegans*

Eva Yezerets EYEZERE1@JHU.EDU
Department of Biomedical Engineering
Center for Imaging Science
Johns Hopkins University
Baltimore, MD 21218.

Noga Mudrik NMUDRIK1@JHU.EDU
Department of Biomedical Engineering
Center for Imaging Science
Johns Hopkins University
Baltimore, MD 21218.

Adam S. Charles ADAMSC@JHU.EDU
Department of Biomedical Engineering
Center for Imaging Science
Mathematical Institute for Data Science
Kavli NDI
Johns Hopkins University
Baltimore, MD 21218.

Abstract

Despite innumerable efforts to characterize *C. elegans* neural activity and behavior, the roles of each individual neuron and the compositional mechanisms of all their interactions are still not completely known. In particular, there is evidence that *C. elegans* neurons perform changing roles over time, in different behavioral contexts, etc.; however, existing stationary anatomical and functional connectivity can average across time and obfuscate the nonstationary nature of the neural dynamics. We contribute to these efforts by leveraging recent advances in decomposed linear dynamical systems (dLDS) models. dLDS models neural dynamics in a latent space with a set of linear operators that can be recombined and reused over time, enabling the discovery of multiple parallel neural processes on different timescales. We leverage the ability to identify reused patterns of dynamical neural interactions, which we call "dynamical connectivity," to 1) identify contextually dependent roles of neurons; 2) discover the underlying variability of neural representations even under discrete behaviors; 3) quantify differences between anatomical, functional, and dynamical connectivity; and 4) learn a single aligned latent space underlying multiple individual worms' activity. These results highlight the importance of defining a neuron's functions not solely by its internal activity or place in a time-averaged network, but by its evolving interactions across context-dependent circuits.

1. Introduction

Using only 302 neurons, *C. elegans* can pirouette, navigate mazes, adapt to stimuli, and even learn associations (Kato et al., 2015; Gourgou et al., 2021; Zimmer et al., 2009; Stein and Murphy, 2014; Flavell and Gordus, 2022). These sensorimotor and cognitive processes all occur in parallel with

other homeostatic functions. How can such a small network of neurons adapt to the worm's complex needs and generate behaviors on short timescales of milliseconds to minutes?

C. elegans is an incredibly well-mapped organism. The anatomical connectome and proposed functions for almost all of its 302 neurons individually are available (Atlas; White et al., 1986; Cook et al., 2019; Witvliet et al., 2021; Randi et al., 2023). While a useful scaffold, the anatomical connectome alone is insufficient to understand the mechanisms by which *C. elegans* implement its complex repertoire of behaviors. In fact, recent work showed a number of discrepancies between the functional connections recorded from pairs of neurons and the activity predicted based on the anatomical path lengths between them (Randi et al., 2023). Moreover, the neuropeptidergic connectome has begun to be mapped (Beets et al., 2022), and its concordance with the anatomical connectome appears limited (Flavell and Gordus, 2022). These findings are consistent with the diversity of signaling mechanisms and timescales. For one, *C. elegans* neurons can communicate both with and without traditional action potentials—consider the nociceptor ASH, which can generate graded responses to stimuli; action potentials in the traditional sense are not required for signaling from ASH to AVA, a key interneuron (Lindsay et al., 2011). For another, pairs of cells can communicate with each other on multiple timescales—from milliseconds across gap junctions, to seconds for action potentials, to minutes across gap junctions again, with neuromodulators concurrently playing a role on the timescale of seconds to minutes—as in the defecation-related pacemaker signal (Jiang et al., 2022; Wang et al., 2013). It is particularly difficult to map function onto the *C. elegans* anatomical connectome because direct, synaptic signaling and long-distance chemical messengers (i.e., neuropeptides) may operate on similar timescales to each other in this species, so either a multi-hop connection directly across neurons or a neuropeptide could reasonably implement a seconds-long functional response that is relevant to a seconds-timescale behavior.

To address this gap in mechanistic understanding, multiple groups have characterized aspects of *C. elegans*' stationary, i.e., time-averaged, functional connectome (Beets et al., 2022; Randi et al., 2023). For example, recent work has described functional connectivity modes via principal component analysis (Atanas et al., 2023), and has used topologically motivated analyses (Uzel et al., 2022) to conclude that the redundancy and flexibility of *C. elegans* neural circuitry means that only perturbing certain hub neurons has a significant impact on function.

However, *C. elegans* generates nonstationary cognitive processes and behaviors. Multiple processes happen on overlapping timescales, including homeostatic processes such as managing energy levels and attention (Kim and Flavell, 2020), and even its most clearly annotated neural pathways are used in slightly different ratios throughout behavioral motifs (Hallinen et al., 2021). Moreover, the species has demonstrated associative and non-associative learning (e.g., habituation, sensitization) (Rankin and Broster, 1992; Rahmani and Chew, 2021) via chemosensation, mechanosensation, and proprioception, with short-term memory shown to persist over minutes (Gourgou et al., 2021) and long-term memory over hours (Stein and Murphy, 2014) to up to a day (Rankin et al., 1990; Rose and Rankin, 2001; Ardiel and Rankin, 2010). Because learning can occur over the course of a minutes-long trial in this species, stationary functional connectomes averaged across trials are meaningful for understanding the general functions of certain networks of neurons, but they are insufficient for understanding how neurons create behavioral changes over the seconds-to-minutes timescale.

Finally, even without nonstationarity, behaviors that appear stereotyped are not completely so; each worm's neural dynamics are unique (Stern et al., 2017). In order to identify shared vs. individual mechanisms of neural signaling across worms, which may have slightly different recorded neurons, trial durations, experimental conditions, and frequencies, durations, and qualities of performed behaviors, it is necessary to have a common framework or space of operators for comparing them.

To track time-varying relationships between cognitive states or processes both within and across individuals, we need dynamical systems models. Such models reinterpret high-dimensional time series data, such as neural population activity, as noisy manifestations of underlying, lower-dimensional processes that evolve within certain constraints in the state space, e.g., on a manifold. The manifold can be shared across individuals, representing a common functional landscape of cognitive processes.

The evolution between latent states can be described by trajectories, i.e., dynamics. With such a model, it is possible to represent latent functional states at each time point and map those back to the neural activity patters for each subject to examine dynamic connectivity.

To date, time-varying models of *C. elegans* neural dynamics have primarily employed switching linear dynamical systems (SLDS) (Linderman et al., 2019; Costa et al., 2019; Randi and Leifer, 2020). Such models assign a single, discrete state to each time point or time window, but the states are nonstationary, unlike in, e.g., dynamic mode decomposition (Brunton et al., 2016). SLDS models are locally linear and hierarchical, with continuous latent states being controlled by discrete overall neural population states. These have shown strong concordance between model-inferred neural states and experimentally-labelled behavioral states. However, such models are limited by the assumption that the entire neural population is experiencing the same overall state, and that these overall states transition abruptly from one to the other.

We address this gap in available modeling frameworks with our recently developed decomposed linear dynamical systems (dLDS) model (Figure 1). dLDS allows for locally linear, nonstationary dynamics that can be active simultaneously in different continuous ratios, and that can transition continuously without such hierarchical state constraints (Mudrik et al., 2024). The coefficients that describe the time-varying utilization of these dynamics can show differences between instances of a behavior within a trial while still containing decodable information about behavior-related latent neural process motifs. The dynamics operators (DOs) themselves describe relationships between latent neural process dimensions that can be mapped back to functional relationships between neurons. Furthermore, these operators can be linearly recombined in different ratios, as regulated by a set of coefficients that capture when different dynamics turn on and to what extent, enabling the modeling of gradual transitions in neural dynamic connectivity throughout behavior.

Using dLDS models learned for individual *C. elegans* (per-worm) models and the across-worm aligned model extension we develop here, we discover the dynamic (i.e., nonstationary, anatomy-unconstrained functional) connectivity maps from learned DOs. These maps represent dynamic connections beyond anatomy or one-to-one direct stimulation-induced stationary functional connections, and reveal key nonstationary properties of neurons in *C. elegans*. For one, the dynamic connectivity maps reveal how stereotyped discrete behavior has a neural basis that, while also patterned, is also variable across repetitions of the same behavior and across individuals. We further show that our model's decomposition of the dynamics underlying these maps disentangles concurrent processes within a trial, such as adaptation to varying aversive oxygen levels while performing a repetitive behavior.

The variability in dynamics underlying discrete behavioral states can highlight functional networks related to latent neural processes that can be otherwise difficult to observe, isolate, and test. These difficulties arise as such circuits can be the result of internal processes separate from the measured behavior and environmental variables, or because they reflect those variables indirectly, e.g., in the form of intermediary computations bridging sensory and behavior. In other words, even when activity levels of a neuron look similar across behaviors, the dynamical connectivity of those neurons with the rest of the network differs, indicating new roles for neurons with and without known functions. We are thus able to characterize the dynamic roles of interneurons such as AVFR, RIS, and RIGL, which more strongly reflect behavior than stimulation state, as well as the sensory BAG neurons, the motor neuron RMED, and the interneuron/motor neuron SABD, which strongly reflect both behavior and stimulation state and the interactions between their levels. These results complement and extend the extensive study of stationary properties of neurons in *C. elegans*, bringing a new analysis of their non-stationary properties.

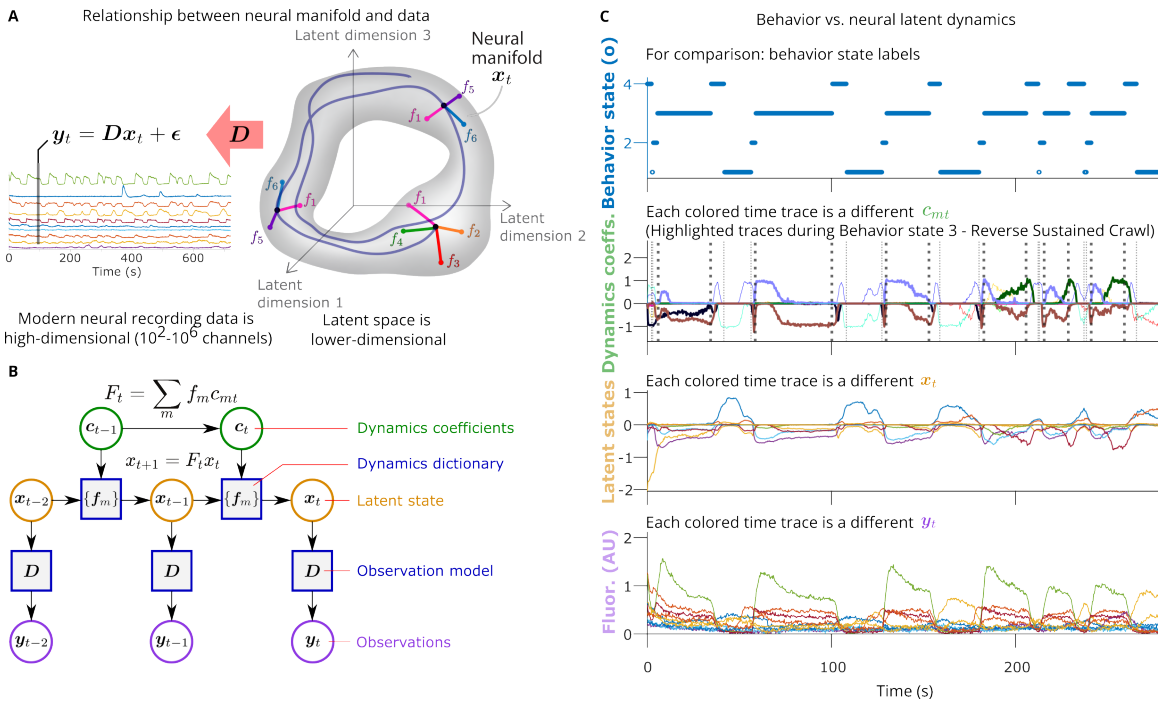

Figure 1: **Modeling latent manifolds from neuroimaging data.A:** Recorded neural activity $\boldsymbol{y}$ relates to latent neural states on the manifold $\boldsymbol{x}$ via observation model (matrix) $\boldsymbol{D}$. Neural dynamics (trajectories) on the manifold operate in the tangent space. These linear operators can be summed linearly. **B:** Graphical model depicting the relationships between data $\boldsymbol{y}$ and model parameters from time point to time point (dynamics coefficients $\boldsymbol{c}$, DO dictionary of matrices $\boldsymbol{f}$, latent states $\boldsymbol{x}$, and observation model $\boldsymbol{D}$). Dynamics coefficients $\boldsymbol{c}$ describe DO use over time. **C:** Sample of time traces of behavior, dynamics coefficients, latent states, and fluorescence data.

2. Results

2.1 dLDS characterizes the discrete and continuous aspects of behaviorally relevant dynamics

First we present the dLDS formulation and how its learned parameters reflect latent, concurrent neural processes through a generative model. In our latent dynamics model, the observed neural fluorescence $\boldsymbol{y}_t$ at time t can be expressed in terms of a set of latent states $\boldsymbol{x}_t$ as $\boldsymbol{y}_t = \boldsymbol{D}\boldsymbol{x}_t$, where $\boldsymbol{D}$ describes to what extent each latent dimension represents each recorded trace and in what combination. In our model, we hold the representation of the latent states $\boldsymbol{D}$ constant for each individual worm. Within the latent space, dLDS models the trajectory of the latent state as a time-varying linear dynamical system, i.e., $\boldsymbol{x}_t = \boldsymbol{F}_t\boldsymbol{x}_{t-1}$. To learn the core dynamical patterns underlying the data, dLDS further models the time-varying system $\boldsymbol{F}_t$ as a linear combination of stereotyped interconnection patterns that drive the full dynamics. Specifically we have $\boldsymbol{F}_t = \sum_{m=1}^{M} \boldsymbol{f}_m c_{mt}$, where the set of M dynamics operators $\{\boldsymbol{f}_m\}_{m=1,\ldots,M}$ are system properties (i.e., interconnection patterns possible in the system) and the coefficients c_{mt} represent which patterns appear at each time t (i.e., when $c_{mt} \neq 0$) and how much influence they have. We refer to the set of $\{\boldsymbol{f}_m\}_{m=1,\ldots,M}$ operators as dynamics operators (DOs) and $c_{mt} \neq 0$ as dynamics coefficients.

Each DO is a matrix that is learned from the data and describes a specific set of latent dimensions that oscillate together in different ratios. DOs represent latent neural processes, and can even be shared across trials or individuals. The DOs are used sparsely by regulating the time-varying dynamics coefficients $\boldsymbol{c}_t$ such that only few, but usually more than one, of the DOs are active at the same time. Experimental model reconstruction performance and parameters are explained in detail in Tables 1 and 2.

A key assumption of interpretability-focused dynamical systems models of neural data is that neural activity is compositional, i.e., that it has its own vocabulary and grammar of how populations of cells interact with each other to produce meaningful, adaptive (behavioral) processes and states. In the case of dLDS, the vocabulary consists of DOs, and the grammar that regulates how they work together to generate latent neural states consists of the dynamics coefficients. Then, we use $\boldsymbol{D}$ to translate from the language of latent states to the language of observable neural activity. Using such dynamical systems models, we can make inferences about the features of systems that generate that neural activity, and therefore the behavior. All neurally-generated variables should be encoded in neural activity; it is more than just a noisy version of discrete behavioral states. Therefore, the learned model parameters should reflect quantitative information such as speed of movement or modulation in response to sensory stimuli, as well as other background cognitive processes, e.g., hunger, wakefulness, etc. Here, we demonstrate dLDS's capabilities to capture these simultaneously active neural processes and variables by characterizing the dynamics of *C. elegans* neural activity.

This *C. elegans* calcium imaging data (Kato et al., 2015) was collected from 12 worms. Five of the worms experienced hyperoxia for 18 minutes (NoStim trials) to spontaneously elicit a pirouetting behavior, i.e., a sequence of forward crawling, turns, and reverse crawling. Seven of the worms were exposed to hyperoxia (21% oxygen) for the first half of the experiment, and alternating bouts of hypo- and hyperoxia (4% vs. 21% oxygen) for the second half in order to entrain the pirouettes to the oxygen levels (Stim trials). Approximately 100 calcium traces were identified from the imaging data per worm. Of these traces only approximately 30 were labeled as originating from one or more known neurons, some with multiple neurons per trace and with some neurons appearing as labels for multiple traces. Moreover, once the protocol was established, the calcium imaging recordings were actually performed in immobilized worms. Despite this limitation (Hallinen et al., 2021), Kato et al. (2015) also provided expert labels for the discrete fictive pirouetting behavioral states by inferring their behavior from the activity of key neurons. These were coarse-grained for the Stim experiments (1: 'FWD' forward crawling, 2: 'REV' reverse crawling, 3: 'REVSUS' sustained reverse crawling, 4: 'TURN' post reversal turn) and fine-grained for the NoStim experiments (1: 'FWD' forward crawling, 2: 'SLOW' forward slowing, 3: 'DT' dorsal post reversal turn, 4: 'VT' ventral post reversal turn,

5: 'REV1' reverse crawling, 6: 'REV2' reverse crawling, 7: 'REVSUS' sustained reverse crawling, 'NOSTATE' - ambiguous). We then applied dLDS to each individual worm's normalized (dF/F) traces.

The dLDS DO coefficients $\boldsymbol{c}$ reflect the utilization of DOs to generate latent neural states. Qualitatively, we had previously observed that the same coefficients appeared in similar patterns during the same behaviors. These combinations of latent processes were discrete in that similar sets of DOs appeared every time, but they were also continuous because they appeared in slightly different ratios which evolved gradually over time or shifted in response to environmental variables such as stimulation protocols without switching completely. To observe these behavior-related encodings in the DO coefficients $\boldsymbol{c}$ more quantitatively, we performed clustering analyses using t-distributed stochastic neighbor embedding (t-SNE) and Isomap, and regression vs. behavioral states using Support Vector Machine (SVM) models. Thus, from the dLDS DO utilization coefficients $\boldsymbol{c}$ and from their first derivative $\frac{d\boldsymbol{c}}{dt}$, it was possible to decode the behavioral state labels inferred by Kato et al. (2015) (Fig. 2 - Stim Worm 1 and NoStim Worm 1 shown in detail; Isomap for $\boldsymbol{c}$ only for all others, Supplementary Figs. 1, 2, 3). (There is some bias due to the base rates of forward and reverse crawling vs. relatively short bouts of turning.) By clustering and coloring by behavioral states, t-SNE appears to show a continuum from forward to backward crawling (DO coefficients first derivative $\frac{d\boldsymbol{c}}{dt}$), while Isomap embedding reveals a ring-like structure from state to state (with additional loops) in the coefficients and a spoke-like structure in the first derivative. By modeling via a classification tree and linear discriminant analysis, it is also possible to classify at least the two major behavioral states from the DO coefficients alone. The observations above were similar when decoding from the latent states $\boldsymbol{x}$. In Sections 2.2 and 2.3, we also investigated the behavioral and environmental context-dependent differences in DO utilization and what the DOs mean in the neural space.

We then proceeded to test the decoding of other additional variables, such as speed or oxygen concentration, from the DO coefficients or latent states. First, we trained an SVM to predict nonstationarity, i.e., whether individual time points were in the first or second half of the trial based on either 1) the DO coefficients ("c vals") or 2) the latent states ("x vals") at only that time point. These SVMs correctly classified at 85% mean accuracy for the DO coefficients and 87% mean accuracy for the latent states (Supplementary Figs. 4, 5). However, we saw slightly decreased mean accuracy (84% for the DO coefficients, 85% for the latent states) in the prediction of precise oxygen levels (detailed stimulation times in the Stim experiments only, rather than first half vs. second half), where 4% oxygen times were primarily misclassified as 21% oxygen (Supplementary Fig. 6). This is not entirely surprising, as it is not possible to change the oxygen concentration in a chamber uniformly and instantaneously, and the base rate of 21% oxygen exposure was higher in these experiments. Despite these confounds, the latent states and DO coefficients are clearly nonstationary between the two halves of all the Stim experiments and 4 out of the 5 NoStim experiments in a way that an SVM can decode (Supplementary Figs. 4, 5). Since nonstationarity was also observed in the NoStim worms, dLDS may be picking up on nonstationarity in the data not only due to the oxygen protocol, but also likely due to other time-dependent factors.

As far as classifying speed (forward crawling vs. forward slowing), SVMs trained on either the DO coefficients or the latent state values were also successful (mean accuracy: 83% for the DO coefficients, 82% for the latent states), but were mostly biased toward the forward slowing states (Supplementary Fig. 7). Overall, we found, qualitatively and quantitatively, that the DO coefficients do encode features of the latent neural states that reflect both the discrete and continuous nature of the behaviors they generate.

2.2 dLDS identifies instantaneous dynamic connectivity between neurons

Having found evidence that the DO coefficients reflect behaviorally-relevant, continuous patterns in the neural activity, we then set out to quantify how the DOs themselves affect the neural activity and connectivity. Given that dLDS DOs transition smoothly, potentially to reflect gradual changes

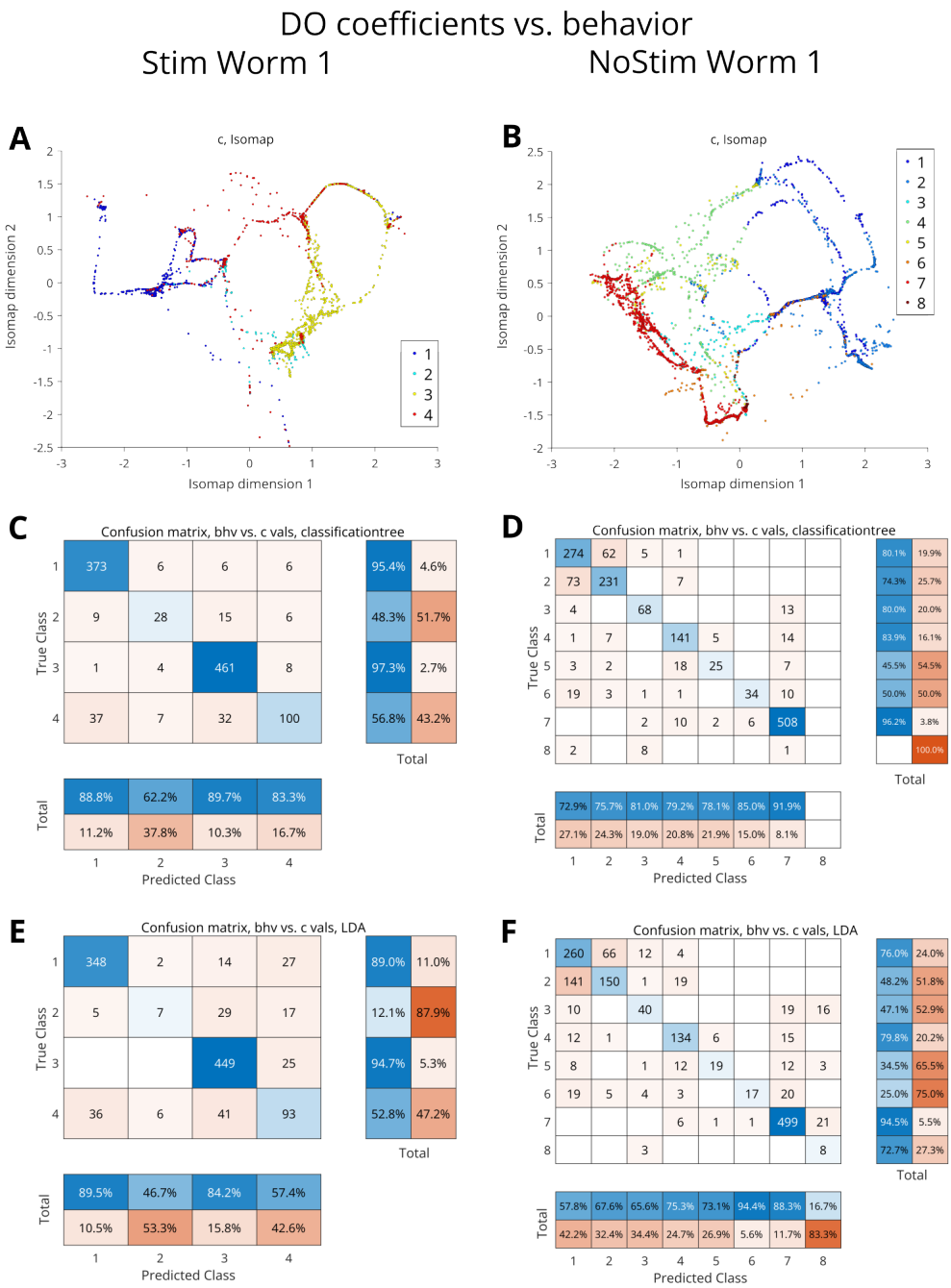

Figure 2: **Decoding dynamics operator coefficients vs. behavior. Left:** Results for Stim Worm 1. **Right:** NoStim Worm 1. **A,B:** Isomap finds a ring-like 2D embedding of the DO coefficients themselves, well clustered by behavior state (more examples in Supplementary Figs. 1, 2, 3). While biased toward the two behavior states with the highest base rates (1-FWD and 3-REVSUS in Stim, 1-FWD and 7-REVSUS in NoStim), both linear discriminant analysis (**C,D**) and classification trees (**E,F**) achieved high decoding performance on the DO coefficients.

in neural activity during or between behavioral states or other time-varying factors, such as oxygen levels, (e.g., Fig. 3, Supplementary Figs. 8, 9, 10, 11, 12, 13), it is important to understand which neurons corresponding to those DOs are active and correlated at each time point in order to interpret the gradual effects of these DOs. We created dynamic connectivity maps that can tie latent states and dynamics operators back to the neural space by simulating the effects of any linear combination of DOs at any time point (or the effects when applied to an impulse function of latent states). The dynamic connectivity maps essentially capture the correlational structure of an equivalent linear time-invariant system with the dynamics coefficients c_{mt} frozen for all time (see Methods Section 6.2). By tracking how the dynamic connectivity maps change over time with the changes in c_{mt} we can track the dynamic networks active across all the recorded neurons.

As described in Section 2.1, the results abounded with occurrences of repeated motifs of simultaneously active DOs (often corresponding to behavior states) that appeared similarly but in slightly different ratios at different times throughout the trial and also gradually evolved during the course of a behavior state. In Figure 3, we show a generative example of the effects of different ratios of two DOs in combination. These two DOs appeared in combination during reverse sustained crawling in Stim Worm 1, but did not merely turn on when the reverse sustained crawling behavior started and turn off when it ended — their dynamics coefficients increased and decreased in magnitude gradually throughout the behavior. We see a small, gradual transition in which neurons participate most strongly as we move from one operator to another — for example, the SABV neurons and RIFR, cholinergic motor/interneurons (Altun, 2014), become less connected and less active. This suggests that while most of the circuit participating in this behavior stays constant throughout the behavior, gradual changes at the neuron interaction level might also occur throughout the course of the behavior. Such continuous changes to the latent dynamics throughout behavior states are perhaps needed to generate preparation to change to the next behavior or other internal processes.

2.3 dLDS identifies nonstationary, superimposed and context-dependent dynamics

Given the alternating hypoxia/hyperoxia oxygen stimulation protocol (second half of the Stim experiments), we investigated if and how some DO coefficients were different in the two halves of the Stim experiments, how the differently-utilized DOs might feature oxygen-sensing neurons in their corresponding dynamic connectivity maps, and how interneurons reflect behavior and stimulation.

2.3.1 BAGL and BAGR neurons and their circuits

The BAG neurons are known to be involved in sensing increased carbon dioxide or decreased oxygen (Altun, 2014; Zimmer et al., 2009; Nichols et al., 2017), so this pair of neurons was a natural candidate for evaluating whether the DOs that were more or exclusively active in the second half of the Stim experiments featured BAG more heavily. There were two possible hypotheses: all DOs might feature BAG relatively equally in order to make them all accommodate for the change in experimental conditions while creating the stereotyped behaviors, regardless of which half of the experiment they were in, or some DOs might feature BAG more strongly in a nonstationary way, possibly to account for hypoxia, separating out the underlying BAG-dependent circuits that are simultaneously active with the circuits that produce the stereotyped behaviors that persist throughout the experiment. This second hypothesis could not be explored with a switched linear dynamical system, where only one operator would represent each state at each time point.

What we found was even more nuanced and supports recent reports of the context-dependent function of BAG (Riedl et al., 2022). In the per-worm models, BAGL and BAGR were strongly present in DOs that were only active in the second half of the trials (alternative oxygen levels) in more than half of the worms and in DOs that were mostly active in the second half in more than a third of the worms (Supplementary Figs. 14, 15, Table 3). Furthermore, they were present in *none* of the operators that were exclusively or mostly in the first half (Supplementary Figs. 16, 17).

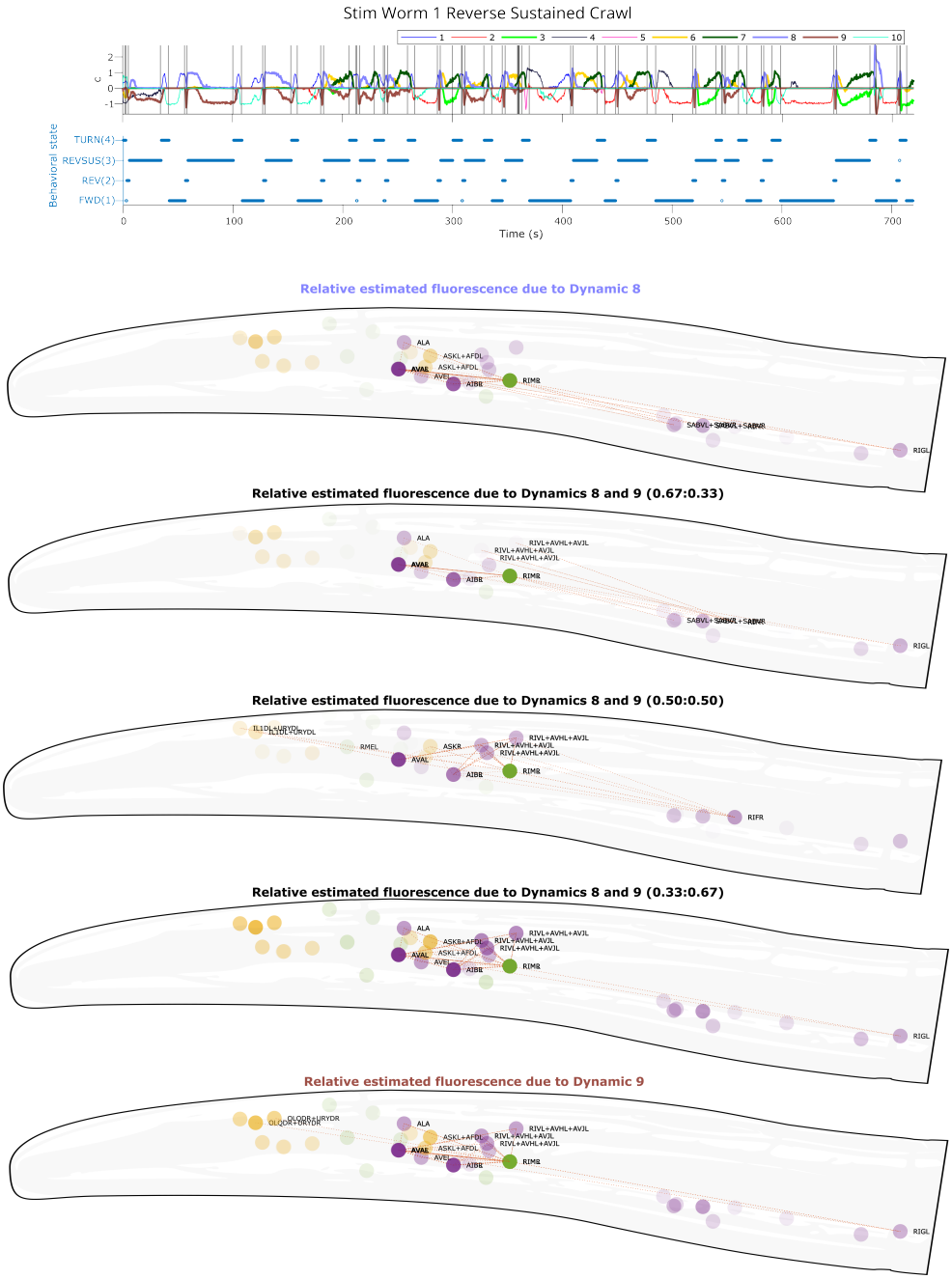

Figure 3: **Continuous transition between DOs during behavior.** DOs 8 and 9 in Stim Worm 1 are active during behavior state 3 (REVSUS). As DO 8 transitions to DO 9, connectivity between a core set of interneurons and the sensory neurons on the head side (left) as well as motor neurons on the body side (right) evolves in terms of which neurons are involved as well as in terms of strength and quantity. Here we show these two DOs linearly combined in different ratios, from 100% DO 8, to 67% DO 8 and 33% DO 9, all the way to 100% DO 9.

We did see evidence that the BAG-featuring DOs are used in a nonstationary way throughout the experiments, potentially in relation to the alternating hypoxia/hyperoxia levels. We also observed that BAG-featuring DOs were only up to approximately half of the DOs active during the two major behavioral states (forward crawling and reverse sustained crawling), which indicates that there might be multiple interrelated but distinct circuits, some of which are BAG-related and some of which are more specific to generating the behaviors, that are active simultaneously, and that dLDS can separate them.

We also observed that BAGL and BAGR were not evenly used between behavioral states; DOs featuring BAGL/R utilized during forward crawling were present in all 7 Stim worms (Fig. 18), but only during reverse sustained crawling in 2 out of 7 worms (Fig. 19). This brings up the question of whether BAGL/R activity and connectivity is dependent on behavioral context. This bias of BAG-featuring DOs toward forward crawling could be a result of the base rates of those two behavioral states, which were biased toward forward crawling in the second half of the experiments, indicating that BAGL/R utilization is independent of behavior and is simply more present during forward crawling because forward crawling occurred more often during hypoxia. However, the bias of BAG-featuring DOs toward forward crawling states could indicate context-dependent BAG utilization. This also called into question whether nonstationarity generally was a side effect of when forward crawling was occurring.

Using χ^2 tests for independence (Table 4) to compare to stimulation protocol settings and behavior states in the Stim worms, we also analyzed the strongest levels of BAGL and BAGR reconstructed connectivity and reconstructed activity at each time point when using the full linear combination of operators as identified by dLDS (Fig. 4, Supplementary Fig. 20 - Stim Worm 1 as an example). First, we compared behavior states to stimulation levels and did not conclusively find that they were dependent. In terms of reconstructed activity ($\hat{y}$), at a weak threshold for "active" (median value), both BAGL and BAGR were most related to state 3 (REVSUS), but at a strong threshold (median plus 3 standard deviations), they were most related to state 1 (FWD). At both levels, they were most active during the second half of the experiments (alternating oxygen stimulation protocol). The stimulation protocol results and the strong threshold results align with the visual observations from the connectivity maps above, which only showed the strongest activity levels and connections. As far as the connections to BAGR and BAGL, the χ^2 test results were inconclusive as far as whether they were dependent on stimulation protocol state, but there were more connections during behavior state 3 (REVSUS).

We then conducted Analysis of Variance (ANOVA) tests for the effects of behavior and stimulation levels on the neural activity and on the connectivity values (MANOVA with the Roy's Largest Root statistic) (Table 5). All of the neurons, including BAGL and BAGR, showed significant effects of Behavior and Stimulation levels on the connectivity to and from across all 7 Stim worms. As far as reconstructed neural activity, BAGL showed consistently significant effects of both the behavior levels, stimulation protocol, and the interaction between the two, whereas the effect of stimulation was insignificant for Worm 2's BAGR activity, despite affecting the connectivity.

2.3.2 RMED neuron

For comparison, we identified another forward crawling-biased neuron, RMED, a motor neuron with limited function documentation in the WormAtlas (Altun, 2014). Shen et al. (2016) proposed that the RME neurons regulate the amplitude of head-bending during locomotion. RMED was utilized in 22/31 forward crawling DOs and during forward crawling in 6/7 Stim worms, but only in 4/36 reverse sustained crawling DOs and during reverse sustained crawling in 3/7 worms (Supplementary Figs. 18, 19, Table 6). RMED-featuring DOs also showed some nonstationarity, in that they were not at all present in the small number of DOs exclusively active in the first half of the experiments and were present in DOs exclusively active in the second half in 4/7 worms, but otherwise they were utilized in a more balanced way between halves of the experiment (Supplementary Figs. 14, 15, 16, 17).

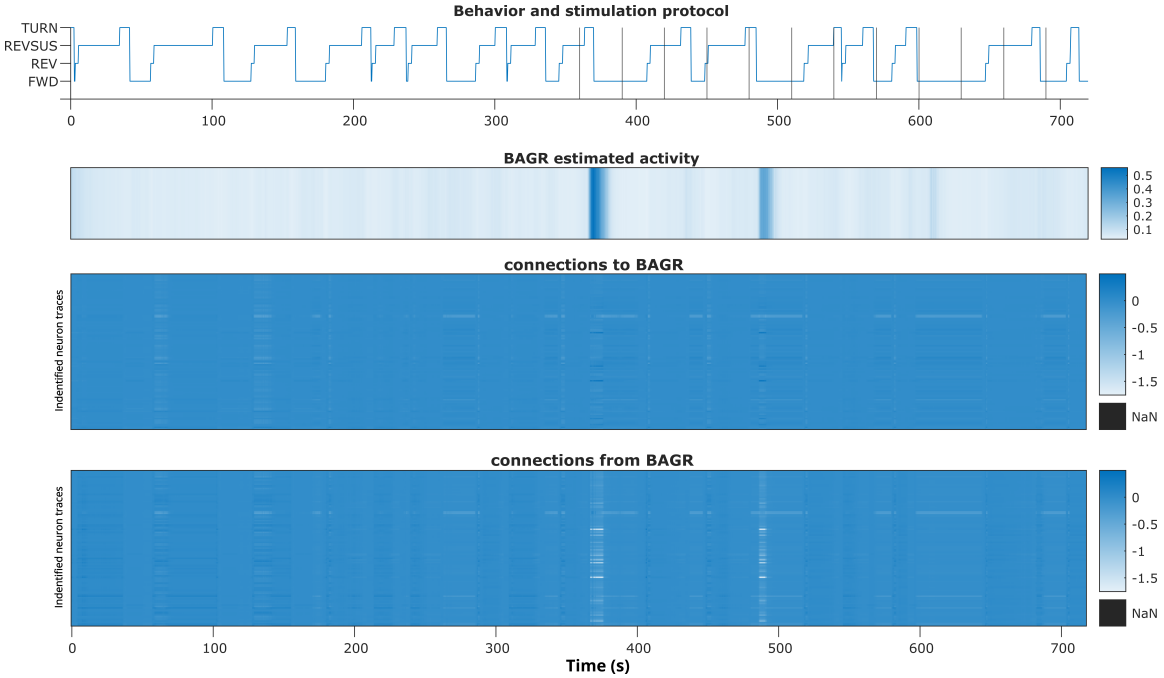

Figure 4: **Reconstructed activity and dynamic connectivity to and from BAGR. Top:** behavior state labels, with vertical lines indicating switches in the oxygen stimulation protocol. **Second from top:** reconstructed BAGR activity ($\hat{y}$). **Bottom two rows:** dynamic connectivity to vs. from BAGR at each time point.

Notably, this relationship between RMED and forward crawling was even stronger in the NoStim worms, which were not exposed to hypoxia. It would seem that RMED should have shown the opposite bias (toward the first half of the Stim experiment) if its nonstationarity were being affected by the oxygenation levels; this observed bias toward the second half of the experiment could be a result of the corresponding bias in the base rates of the forward crawling state(s). To further complicate the story, the χ^2 tests on the reconstructed connectivity and activity of RMED showed weak effects of the stimulation protocol, which is consistent with the findings above, but strong evidence of connectivity during behavior state 3 (REVSUS) and (weakly-thresholded) activity during behavior state 1 (FWD) (Supplementary Fig. 21 - Stim Worm 1 as an example). As with BAGL and BAGR, the ANOVA results showed significant effects of behavior and usually significant effects of the stimulation setting. A possible mechanistic interpretation of the significant stimulation effects is that RMED appears to play a more direct role in sensorimotor circuits than otherwise previously indicated.

2.3.3 Other neurons for comparison: AVFR, RIGL, RIS, SABD

We selected four interneurons—AVFR, RIGL, RIS, and SABD—for further analysis based both on their limited function documentation in the Worm Atlas (Altun, 2014) and on the consistency with which they were uniquely and distinctly labelled across the 7 worms (AVFR in all 7, RIS in worms 1-6, RIGL in worms 2,3,4, and 6, and SABD in worm 1; See Supplementary Figs. 22, 23, 24 for the activity and connectivity of the Stim Worm 1 neurons). Through an ANOVA analysis, we show less consistently significant effects of oxygen stimulation on AVFR, RIS, and RIGL activity, but persistently significant effects on connectivity (Table 5). Furthermore, RIGL showed an instance of less significant interaction term effects on activity. SABD was unique: it is both an interneuron and a motor neuron, and it showed significance for behavior, stimulation, and their interaction term on activity. However, it was only tested for one worm. We interpret these interneuron results to indicate that the more interneuron-like an interneuron is, the more its activity appears isolated from external variables (e.g., oxygen levels), even though the connectivity may still be modulated in relation to them.

2.4 dLDS dynamic connectivity maps identify novel connections compared to stationary anatomical and functional connectivity atlases

While the *C. elegans* anatomical connectome has been available for over a decade (Atlas), questions remain as to context-dependent functions, nonlinear relationships, and differences between individuals in terms of how those neurons work together. More recently, the pairwise stationary functional connectome has been mapped by stimulating each neuron and observing the responses of every other neuron individually (Randi et al., 2023). Along with greater understanding of the role of long-range neuropeptide signaling, this functional connectome work has revealed novel relationships that are not mediated by direct synapses.

Using dLDS, we investigated dynamic connectivity, which we define as the graph where each vertex is a single neuron and each edge from nodes i to j is the directional local influence of neuron i on neuron j. As dLDS is a non-stationary model, this definition of connectivity allows each edge to be time-varying and to capture the changes in network structure across behaviors. Moreover, the ability of dLDS to represent nonlinear dynamics can further capture effects such as two or more neurons needing to be active to activate another downstream neuron (AND gate)—an effect that cannot be determined from one-to-one stationary functional connectomes.

We compared the dynamic connections found by the subset of *C. elegans* head neurons recorded in this dataset to the aforementioned anatomical and functional connectomes. The magnitudes of dynamic connections that were also found in the respective reference were kept positive (red), while connections that were unique to the dLDS model were given a negative coefficient (blue). We observed that, across the Stim and NoStim worms, a majority of the connections identified by dLDS

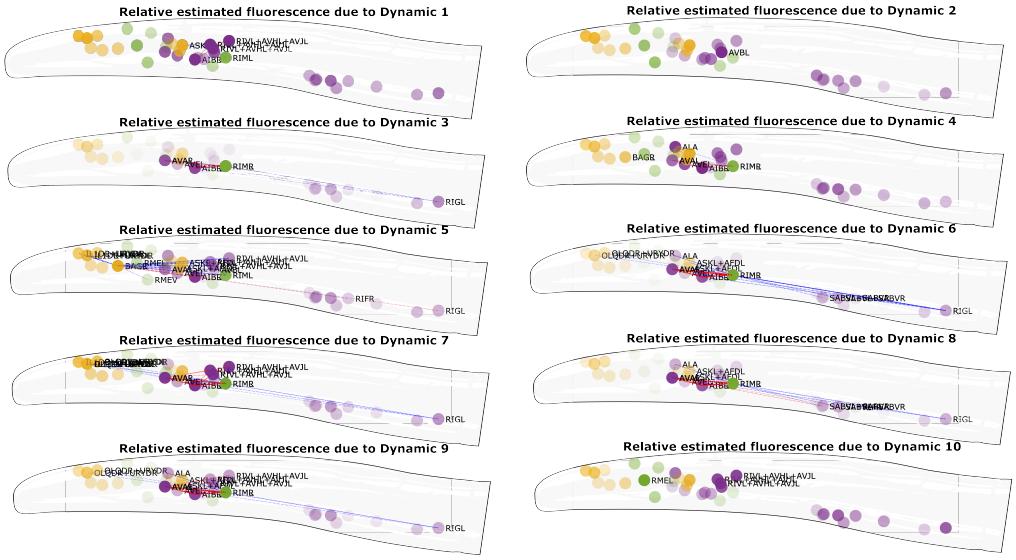

Figure 5: **Dynamic vs. anatomical connectivity, Stim Worm 1.** As red lines, we show connections that are identified both by the Worm Atlas (Atlas) and by dLDS; in blue, we show novel connections identified by dLDS. Dots are known neurons, where opacity denotes simulated, time-averaged neural activity and color denotes neuron class (yellow: sensory, purple: motor, green: interneuron).

did not match those in the anatomical or functional connectivity reference atlases, although some connections did (Figs. 5, 6, Supplementary Figs. 25, 26, 27, 28). These dLDS-only connections could be avenues for future exploration.

2.5 dLDS enables the alignment of latent manifolds across individuals

While per-worm models are useful for characterizing the dynamics of individual worms and even show some commonalities in terms of the dynamic connectivity maps across worms corresponding to different behavioral states or environmental variables, we wanted to investigate how a *shared* latent neural manifold might reflect more general principles of dynamic connectivity across worms. We modified dLDS to learn one set of DOs across all 7 Stim worms, with an individual observation matrix for each worm, resulting in one aligned model per worm (Fig. 7). We kept all the same hyperparameters as for the individual models, with the exception of allowing 70 DOs (thus permitting the possibility of 10 completely unique operators per worm).

We found that, while the aligned models' inferred DO coefficients were sparser than the total possible number of DOs, they were usually less sparse than the per-worm models (Supplementary Figs. 8, 9, 13). As each worm had a different projection out from the latent space (i.e., the per worm representations $\boldsymbol{D}$), we sought to understand potential differences in neural representations among worms related to the same DO in the latent state. Specifically, does the same DO have a different "meaning" in terms of neuron-space dynamic connectivity across worms (e.g., DO 29 in Supplementary Figs. 29, 30, and correlations between DOs vs. coefficients in Supplementary Figs. 31, 32)? We thus tested whether the aligned DOs were washing out any structure, splitting

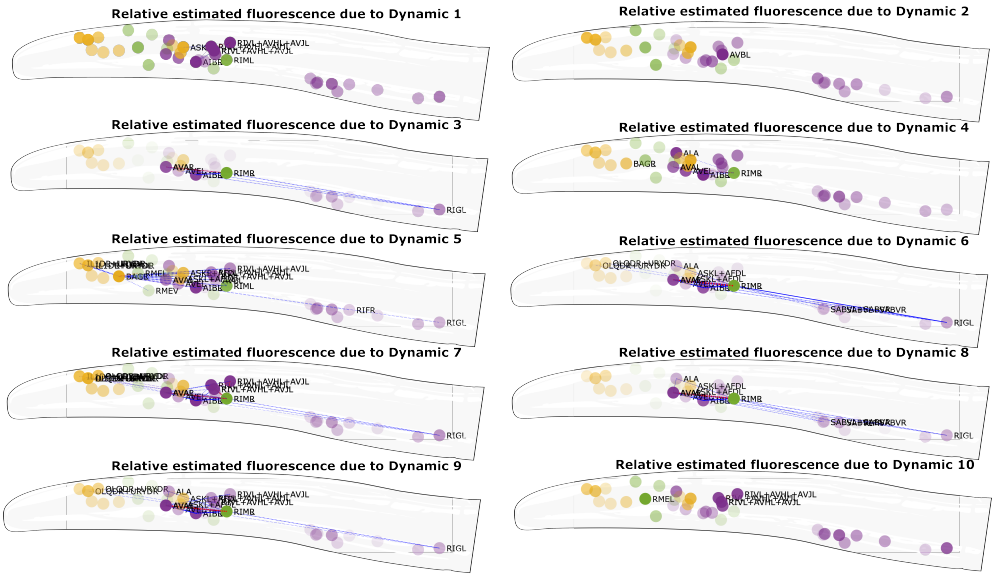

Figure 6: **Dynamic vs. stationary functional connectivity, Stim Worm 1.** In red we show connections that are identified both by Randi et al. (2023) and by dLDS; in blue, we show novel connections identified by dLDS. As in Figure 5, dots are known neurons, where opacity denotes simulated, time-averaged neural activity and color denotes neuron class (yellow: sensory, purple: motor, green: interneuron).

up dynamic connectivity maps in space, or subdividing the activity of the per-worm operators in time, reflecting nonstationarity in a finer-grained way. By tallying features of the aligned DO dynamic connectivity maps (e.g., BAG and RMED participation), we observed that the aligned model operators shared key dynamic connectivity map features with the per-worm models. Therefore, even though the aligned model DOs used the same directions on the shared manifold to generate different connectivity maps, the aligned DOs overall for each worm still captured important and similar trends in which neurons were coactive and the relationships between them through time (e.g., Supplementary Figs. 19, 30). We also observed smooth transitions in the middle of behavioral states in the aligned models, reminiscent of those in the per-worm models. This led us to reject the hypothesis that the aligned model with 70 DOs was washing out structure entirely.

Then, for each pair of per-worm and aligned DO coefficient traces, we calculated the probability of the intersection of their activity divided by the activity of one of the two DOs (e.g., Stim Worm 1, Supplementary Fig. 33). We saw a marked asymmetry: each aligned DO represented a small percentage of a per-worm DO utilization probability, but whenever an aligned DO was active, it was strongly coactive with at least one per-worm DO, and sometimes multiple. This indicated that the aligned DOs split up the per-worm DOs utilization patterns in time, as well as subdividing and reusing in multiple ways the dynamic connectivity maps associated with the per-worm DOs. In conclusion, when aligning dynamics across individuals using dLDS, model size can have an impact on how key dynamics are split up and represented, but the key dynamics will still be decipherable and will still represent key latent neural processes such that shared activity patterns across individuals are preserved.

3. Discussion, Limitations, and Future Work

Here we use the recently developed framework of decomposed linear dynamical systems (dLDS) to uncover simultaneous time-varying neural processes co-occurring during a sensorimotor *C. elegans* behavior. By interpreting directional dynamics in the latent state via their effects in the natural neural space, we reveal evidence in "whole brain" *C. elegans* calcium imaging data (Kato et al., 2015) of context-dependent BAG neuron sensitivity that was only recently shown experimentally (Riedl et al., 2022), and we highlight context-dependent activity of neurons, such as the RME neurons that may be a target for further experimentation.

In general context-dependent functions or nonlinear relationships between neurons has been a challenging endeavor in systems neuroscience. Specifically, context-dependent relationships can overlay and interact with context-independent operators, interacting in ways that would be impossible to unwravel in current RNNs or switched dynamical systems. We demonstrate that exploring the neural interactions through the dLDS dynamic connectivity maps across behavioral states or conditions can reveal these context-dependent functions or nonlinear relationships. Using the dLDS-derived dynamic connectivity, we identified many novel connections not mapped by direct anatomical synapses or one-to-one functional connections, emphasizing the possibility that neurons also communicate indirectly and nonlinearly with other neurons (e.g., as AND, OR, XOR gates, etc.). Moreover, we developed an extension to dLDS that allows latent neural processes to be aligned across individuals. This model extension enables greater generalizability of the learned models.

Our analysis' unique perspective results in the following hypotheses: **Predictions:**

- All of the neurons highlighted in this paper (sensory neurons BAGL and BAGR, interneurons AVFR, RIGL, RIS, interneuron/motor neuron SABD, and motor neuron RMED) are active and connected in a behavioral and environmental context-dependent way. The effects of the environmental context (oxygen stimulation protocol) are most consistent in the sensory and motor neurons, and are less consistently significant in the interneurons.

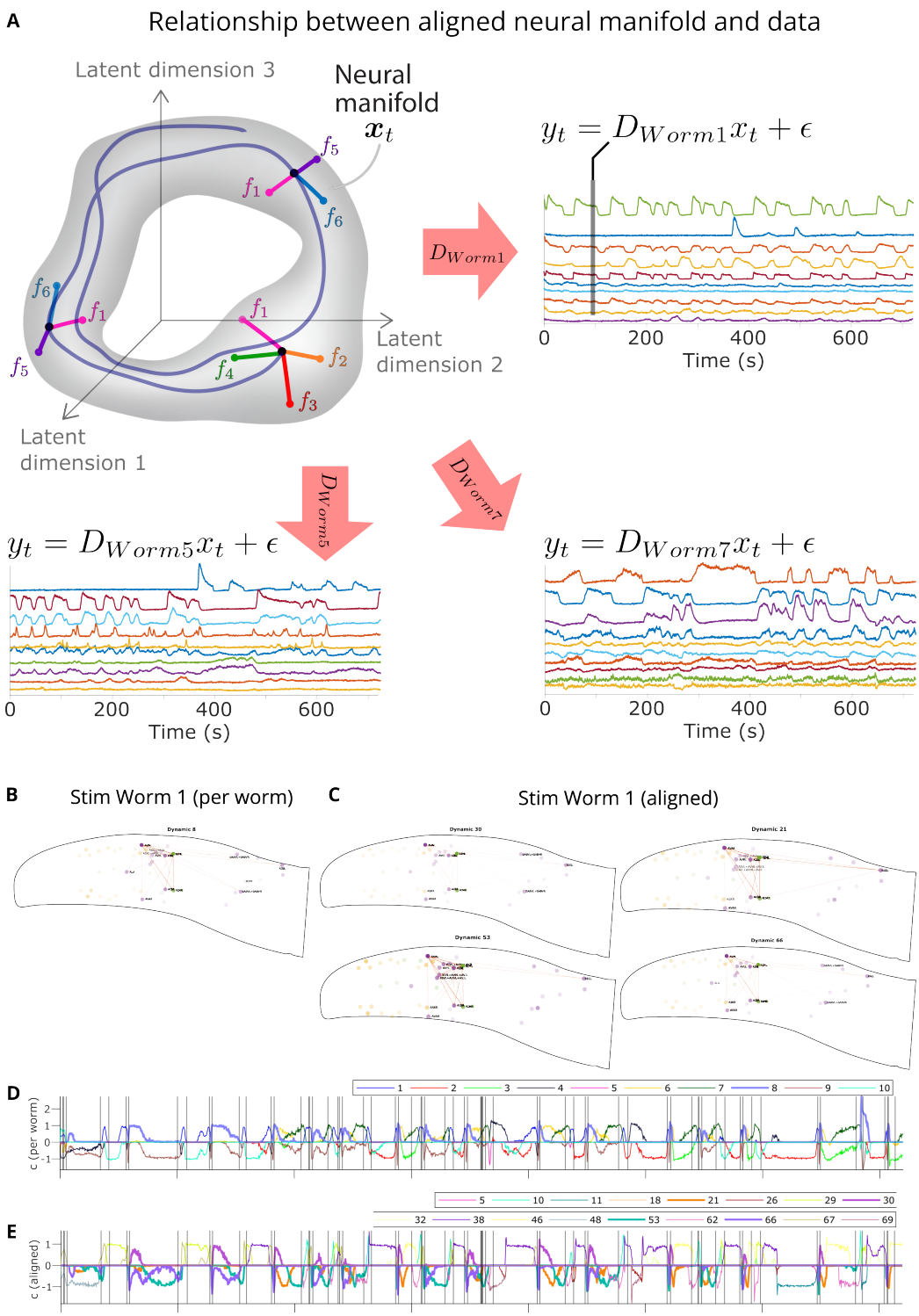

Figure 7: **Aligned latent manifold and Stim Worm 1 example. A:** We learn a shared set of DOs and latent dimensions, but a unique observation matrix and set of latent states and DO coefficients for each worm. **B,C:** We compare the connectivity maps for DO 8 in the per-worm model and the aligned DOs that co-occur with it. **D,E:** The DO coefficients themselves.

- While we expected BAGL and BAGR to be more sensitive to oxygen levels than to behavioral context, the effects of both variables on the connectivity are consistently significant, and behavior has a more consistently significant impact on the activity than does stimulation level.
- Dynamic connectivity maps and the sign of reconstructed connections can highlight periods of neural activity suppression, potentially via inhibition.
- Behaviorally- and environmentally-relevant changes to connectivity can happen without obvious changes to activity, especially in interneurons.
- Dynamic connectivity maps can be used to uncover functional, context-dependent, time-varying, nonlinear, and indirect relationships between neurons, including those such as RMED without well-documented functions, or interneurons with complex, time-varying functions across circuits.
- dLDS-inferred dynamics coefficients can be used to decode behavior, and perhaps other experimental variables as well, from neural activity.

Testing these hypotheses can further establish the contextual time-varying neural activity patters and can accomplished with perturbation experiments, e.g., using a mixture of new protocols and optical stimulation.

In all of our neuron analyses, the activity and connectivity can be decoupled due to how the model's DO coefficients interact with each other. Specifically, underlying changes in connectivity may not necessarily be reflected in obvious changes in activity in every neuron, especially the interneurons. For example, the MANOVA analyses for the relationship between behavior, oxygen stimulation, and connectivity to and from each neuron were always significant, but the ANOVA analyses sometimes returned insignificant effects for the reconstructed neural activity. If looking for a mechanistic explanation, we may propose inhibition in these cases. Indeed, most of the connection values appear to be negative. Moreover, the stronger second-half bias of BAG-featuring DOs could be highlighting an additional, true nonstationary BAGL/R response to hypoxia, not just to the base rates of forward crawling, while still being context-dependent on forward crawling to be active because, as Riedl et al. (2022) showed, BAG neurons recognize self-produced carbon dioxide when crawling backward and their response is suppressed.

Taken together, our results show that dLDS can be used to reveal a detailed story of latent neural processes such as sensation that are overlaid on those latent neural processes regulating motor behavior states, and the complex roles of interneurons in between. We can use dLDS to gain insight into internal cognitive processes that are otherwise difficult to disentangle. While not explored in this study due to the confounding variable of behavior base rates potentially impacting nonstationarity in addition to environmental variables, it is possible that the amplitude of DO coefficients might reflect habituation or sensitization to a sensory stimulus, evidence accumulation, a change in wakefulness or attention, etc. Future attempts at applying dLDS to neural data to interpret quantitative differences in the DO coefficients would also benefit from detailed, quantitative measures of behavior and environment variables.

We would also like to highlight worm individuality. Despite the many features shared by these worms, their similar responses to stimuli, and the similar reconstruction performance achieved by the per-worm and aligned dLDS models, the data were nevertheless not identical and no aligned model used the same model parameters or coefficients in the same way. Moreover, different connections to the BAG neurons were strongest during reverse sustained crawling in each worm (with the most frequent neuron group involved being the RME motor neurons, but also multiple other motor and interneurons).

More generally, dLDS complements the space of current models by enabling both interpretability and expressivity. Switched LDS models can model nonstationary processes in terms of temporally local linear systems, but only one system can be active at a time. dLDS enables the flexibility to put together a combination of linear operators, which allows us to track continuously varying changes in

the network even with single behavioral bouts. Moreover, it allows the modeling of simultaneous parallel processes, such as if an animal is monitoring for potential threats while also navigating its environment for food—or in our case turning while being puffed with oxygen.

4. Data and Code Availability

The code for both the discrete and the continuous models can be found at https://github.com/dLDS-Decomposed-Linear-Dynamics. The discrete code can also be pip-installed using the **dLDS-discrete** Python package, as described in `https://pypi.org/project/dLDS-discrete-2022/`. Additionally, an interactive Python notebook of the discrete model visualization is available at `https://colab.research.google.com/drive/1PgskOtYoLL83ecXz_ALXk9oLofR2AeRf?usp=sharing`.

Data from Kato et al. (2015) were obtained from Zimmer (2021). The SSM Python package from the Linderman lab was used to run rSLDS (Linderman et al., 2020).

5. Acknowledgments

This work was supported in part by NSF grant CCF-1409422, James S. McDonnell Foundation grant number 220020399, the Georgia Institute of Technology, and Johns Hopkins University. Thank you to Sue Ann Koay for the original version of the manifold illustration in Figure 1. Thank you to Francesco Randi for the advice on how to use the Leifer Lab repositories.

6. Methods

6.1 Decomposed Linear Dynamical Systems (dLDS)

In our framework (Mudrik et al., 2024), we rely on the neural manifold hypothesis, that is that neural activity comes from an underlying low-dimensional space that evolves characteristically in time via trajectories, i.e., dynamics. We observe neural activity during behavior as neural time series traces $\boldsymbol{y} \in \mathbb{R}$, which are modeled as a linear function of the latent neural states $\boldsymbol{x}$ via the observation matrix $\boldsymbol{D}$. (Note that here we define a neural latent "state" as a larger process in the brain that can occur simultaneously with other processes, i.e., states, as opposed to one whole-brain or whole animal state at a time.) If trajectories in latent space are a useful model of neural processes, it is necessary to understand them as traversing a manifold. If we look at the tangent space at each latent state time point, we can break down the dynamics trajectories into a linear combination of operators G in continuous time. However, the matrix exponential becomes cumbersome to compute with even a small number of dimensions, so we use the discrete time approximation of this model to work with real neural data.

dLDS uses an expectation maximization algorithm to alternate between jointly inferring the latent states $\boldsymbol{x}$ and the dynamics coefficients $\boldsymbol{c}$, and updating the randomly initialized dynamics dictionary $\boldsymbol{F}$ and observation matrix $\boldsymbol{D}$ via projected gradient descent. Inputs from the user are just the neural activity $\boldsymbol{y}$ and some parameters, including the hypothesized latent dimensionality and number of operators, as well as some regularization terms for sparsity and smoothness of the latent states and dynamics (Table 2). Sparsity is important because it helps with interpretability – it constrains the model to use a small number of linear operators to represent each time point.

1. Randomly initialize $\boldsymbol{F}$ and $\boldsymbol{D}$.

2. Infer $\boldsymbol{x}$ and $\boldsymbol{c}$ via LASSO (Equations 1 and 2):

$$\boldsymbol{x}_t = \boldsymbol{F}_t \boldsymbol{x}_{t-1} = \sum_{m=1}^{M} c_{mt} \boldsymbol{f}_m \boldsymbol{x}_{t-1} = \sum_{m=1}^{M} [\boldsymbol{f}_m \boldsymbol{x}_{t-1}] c_{mt} = \widetilde{\boldsymbol{F}_t} \boldsymbol{c}_t, \tag{1}$$

$$\widehat{\boldsymbol{x}}_t, \widehat{\tilde{\boldsymbol{c}}}_t = \arg\min_{\boldsymbol{x}_t, \boldsymbol{c}_t} \left[\|\boldsymbol{y} - \boldsymbol{D}\boldsymbol{x}_t\|_2^2 + \lambda_0 \left\| \boldsymbol{x}_t - \operatorname{expm}\left(\sum_{l=1}^{L} \boldsymbol{g}_l \tilde{c}_{lt} \right) \widehat{\boldsymbol{x}}_{t-1} \right\|_2^2 \right.$$
$$\left. + \lambda_1 \|\boldsymbol{x}_t\|_1 + \lambda_2 \|\tilde{\boldsymbol{c}}_t\|_1 + \lambda_3 \|\tilde{\boldsymbol{c}}_t - \widehat{\tilde{\boldsymbol{c}}}_t\|_2^2 \right]. \quad (2)$$

3. Update $\boldsymbol{D}$ and $\boldsymbol{F}$ via projected gradient descent (Equations 3, 4):

$$\widehat{\boldsymbol{D}} \leftarrow \Pi_{C_D}(\boldsymbol{D} - \eta_D \nabla_{\boldsymbol{D}} \sum_{t=1}^{T} (\boldsymbol{y}_t - \boldsymbol{D}\boldsymbol{x}_t)^2) = \Pi_{C_D}(\boldsymbol{D} + \eta_D \sum_{t=1}^{T} (\boldsymbol{y}_t - \boldsymbol{D}\boldsymbol{x}_t)\boldsymbol{x}_t^T)), \quad (3)$$

$$\widehat{\boldsymbol{f}}_m \leftarrow \Pi_{C_{f_m}} \left(\widehat{\boldsymbol{f}}_m - \eta_f \nabla_{f_m} \sum_{t=2}^{T} \left\| \boldsymbol{x}_t - \sum_{m=1}^{M} \boldsymbol{c}_{mt} \boldsymbol{f}_m \boldsymbol{x}_{t-1} \right\|_2^2 \right) \quad (4)$$

$$= \Pi_{C_{f_m}} \left(\widehat{\boldsymbol{f}}_m + \eta_f \sum_{t=2}^{T} \left(\boldsymbol{c}_{mt} \left(\boldsymbol{x}_t - \widetilde{\boldsymbol{F}}_t \boldsymbol{c}_t \right) \boldsymbol{x}_{t-1}^T \right) \right). \quad (5)$$

4. Repeat steps 2 and 3 until $\boldsymbol{D}$ and $\boldsymbol{F}$ each converge.

In the aligned model, we modify this procedure by inferring and storing $\boldsymbol{x}$,$\boldsymbol{c}$, and $\boldsymbol{D}$ separately for each worm on each update iteration, whereas $\boldsymbol{F}$ is updated using a cell array containing the data from all of the worms, essentially concatenated as one trial after another.

We applied dLDS to each worm delta fluorescence trace individually on the CIS cluster. Preprocessing was minimal - negative values (up to 3% of each trace) were set to 0 because calcium-based imaging is a non-negative measure of activity. All values were scaled between 0 and 1 (maximum fluorescence value per worm) to promote even reconstruction performance.

Model type	Protocol	Worm number	R^2
Per-worm	Stim	1	0.86
		2	0.78
		3	0.83
		4	0.79
		5	0.79
		6	0.81
		7	0.7
Aligned	Stim	1	0.87
		2	0.84
		3	0.85
		4	0.82
		5	0.75
		6	0.8
		7	0.83
Per-worm	NoStim	1	0.85
		2	0.86
		3	0.81
		4	0.85
		5	0.77

Table 1: **dLDS performance in terms of R^2.**

We first ran 3000 iterations of dLDS and observed that after 500 iterations, all of the models achieved change in $\boldsymbol{D}$ and change in $\boldsymbol{F}$ on the order of 10^{-3}. $\boldsymbol{D}$ and $\boldsymbol{F}$ were stored and used to perform inference one last time after dynamics learning to obtain the latent states ($\boldsymbol{x}$) and dynamics coefficients (c). The number of latent dimensions and dynamics were initialized heuristically as 10 because there were 4-8 behavioral states labelled and because the median number of dynamics active at a time converged to 3-8 with a range of dimensionalities (6, 8, 10, 20), so an intermediate value (10) was chosen in favor of the smallest stable number of coefficients without artificially constraining the median number of active coefficients at any given time (Table 2). Similarly, a range of regularization parameters was explored (from near 0 to greater than 1) before settling on the fairly strong regularization for the smoothness of the states and coefficients. Since $\boldsymbol{D}$ and $\boldsymbol{F}$ are randomly initialized, multiple examples were generated for three of the worms and compared visually.

Parameter	Meaning	How to set	C. elegans parameters (per-worm models)
nF	number of dynamics operators (DOs)	First set to 2x the number of PCs required for 95% variance explained. Then decrease until the median number of active dynamics coefficients starts decreasing. (Goal: minimize the number of DOs while maintaining the inherent dimensionality of the data.) Alternative heuristic: use the number of known behavioral states as a benchmark and double it to get the starting point for the number of DOs, and then start decreasing from there.	10
N	number of latent dimensions	Set approximately equal to nF	10
lambda_val	regularization: sparsity of states (x)	Increase to reduce the number of states active at the same time (moderately sensitive)	0.1
lambda_history	regularization: smoothness of states (x)	Increase to encourage states to change smoothly from time point to time point (less sensitive)	0.9
lambda_b	regularization: sparsity of dynamics coefficients (c)	Increase to reduce the number of DOs active at the same time (sensitive)	0.01

lambda_historyb	regularization: smoothness of dynamics coefficients (c)	Increase to encourage DO coefficients to change smoothly from time point to time point	0

Table 2: **Meaning of key dLDS parameters, heuristics for setting them, and settings used for *C. elegans* models.**

rSLDS was also run for 500 iterations on each worm with 10 latent dimensions and 4 output states for the Stim worms (or 8 for the NoStim worms).

For the reconstructions (Table 1), the product of D with the latent states was rescaled back to the original dF/F range (R^2 between 0.7 and 0.9 for each of the worms). The dynamics coefficients were also compared in terms of their utilization during the experimental settings of the experiment (histograms) and during various behavioral states.

6.2 Computing dynamic connectivity

Each labelled neural trace was matched to a three-dimensional location in the worm and a class, as labelled by Randi et al. (2023). The connections between neurons were calculated as a covariance matrix between traces (from rows to columns). Recall that in a latent dynamics model where $\boldsymbol{y}_t = \boldsymbol{D}\boldsymbol{x}_t$, $\boldsymbol{D}$ is the mapping from the latent space to the ambient (e.g., neural recording) space. In typical connectivity maps, the system (i.e., $\boldsymbol{F} = \sum_{m=1}^{M} \boldsymbol{f}_m \boldsymbol{c}_m$) is considered stationary, but because of the time-varying DO coefficients $\boldsymbol{c}_t$ in dLDS, the system can be modeled in a time-dependent way. Our dynamic connectivity maps can show not only the dynamic (i.e., time-varying) connectivity (via lines between neurons), but also the reconstructed time-averaged or instantaneous activity of those neurons (via neuron opacity) resulting from that particular linear combination of DOs. For any linear combination of DOs $\boldsymbol{F}$, the correlations in the ambient space of an equivalent linear time-invariant dynamical system are calculated as $\boldsymbol{D} * \boldsymbol{F} * \boldsymbol{D}^T$. To produce the time-averaged simulated fluorescence values $\hat{\boldsymbol{x}}$ generated only by a particular combination of DOs of interest, simulated latent states were calculated by applying an impulse function (vector of ones) to the combined DO $\boldsymbol{F}$, taking the dot product iteratively for 500 time points, and then taking the mean reconstructed neural activity for each neuron. To produce stable combined DOs, $\boldsymbol{F}$ was rescaled to unit norm (after linearly combining the component DOs, but before applying the impulse function). Then the simulated latent states were multiplied by $\boldsymbol{D}$ to produce the simulated fluorescence.

The dynamic connectivity maps were produced for only the labelled traces (less than 50% of the recorded traces). If multiple neurons were present in that trace, the activity of that trace was plotted redundantly in each of the locations associated with the corresponding component neurons. The simulated fluorescences plotted were the mean for each trace. Strong thresholding on both the fluorescence values and the connectivity was performed to declutter the plotting - i.e., only the strongest 0.1-0.5% of connections are shown. Thresholding was also performed on the automatic neuron trace labels so that the strongest activity and strongest connections were labelled.

6.3 BAGL/R dynamic connectivity tally

For each behavior or experimental condition context analyzed, the corresponding active DO traces were visually selected for each worm model. Then a dynamic connectivity map was made for each trace, and the presence of key neurons was tallied across those maps, both in terms of their appearance in DOs across worms and whether they appeared in each worm model (Tables 3, 6).

Table 3 is a tally of strong connectivity with or activity in BAGL and/or BAGR across the worms' dynamic connectivity maps for each DO.

subset	per-worm DOs	worms	aligned DOs	worms
Stim FWD	11/31	7/7	24/46	7/7
Stim REVSUS	3/36	2/7	10/54	3/7
Stim only 1st half	0/3	0/7	1/6	1/7
Stim mostly 1st half	0/11	0/7	2/8	1/7
Stim mostly 2nd half	4/8	3/7	3/9	3/7
Stim only 2nd half	8/9	5/7	13/20	6/7
Stim sign flip between halves	1/3	1/7	1/1	1/7

Table 3: **Tally of BAGR or BAGL presence in dynamic connectivity maps across conditions**.

6.4 χ^2 tests

In order to test the independence of individual neuron activity and connectivity levels (on/off) from categorical variables such as oxygen stimulation settings and behavior states, we conducted χ^2 tests (Axensten, 2007) for each Stim worm per-worm model (Table 4). Most tests were found to be significant (i.e., show evidence of neuron dependence on the categorical variable in question), even when the alpha value for rejection was set at an extremely conservative 9e-5, or approximately 1e-4, based on a Bonferroni correction from 0.05 by the number of tests per worm.

Stim worm	variable 1	variable 2	p value	max level
1	bhv	BAGLconnFrom	0.00021448	3
1	FWD	BAGLconnFrom	0.003698056	2
1	Stim	BAGLconnFrom	1.52E-06	2
1	StimDetailed	BAGLconnFrom	7.71E-08	1
2	bhv	BAGLconnFrom	0.852212912	1
2	FWD	BAGLconnFrom	0.374550595	1
2	Stim	BAGLconnFrom	0.316950581	2
2	StimDetailed	BAGLconnFrom	0.563219514	1
3	bhv	BAGLconnFrom	0	1
3	FWD	BAGLconnFrom	0	1
3	Stim	BAGLconnFrom	0	1
3	StimDetailed	BAGLconnFrom	9.35E-05	1
4	bhv	BAGLconnFrom	4.35E-05	3
4	FWD	BAGLconnFrom	0.073295159	2
4	Stim	BAGLconnFrom	0.013499087	2
4	StimDetailed	BAGLconnFrom	0.013105985	1
5	bhv	BAGLconnFrom	0	3
5	FWD	BAGLconnFrom	0	2
5	Stim	BAGLconnFrom	0	1
5	StimDetailed	BAGLconnFrom	0	1
6	bhv	BAGLconnFrom	0	3
6	FWD	BAGLconnFrom	0.001783874	2
6	Stim	BAGLconnFrom	4.38E-10	2
6	StimDetailed	BAGLconnFrom	0	1
7	bhv	BAGLconnFrom	0	3
7	FWD	BAGLconnFrom	0.001913865	2
7	Stim	BAGLconnFrom	0.002194872	1
7	StimDetailed	BAGLconnFrom	0.148005847	1

1	bhv	BAGLconnFrom3	0	1
1	FWD	BAGLconnFrom3	0	1
1	Stim	BAGLconnFrom3	0	2
1	StimDetailed	BAGLconnFrom3	0	1
2	bhv	BAGLconnFrom3	0	3
2	FWD	BAGLconnFrom3	0	2
2	Stim	BAGLconnFrom3	2.22E-16	1
2	StimDetailed	BAGLconnFrom3	2.44E-15	1
3	bhv	BAGLconnFrom3	0	1
3	FWD	BAGLconnFrom3	0	1
3	Stim	BAGLconnFrom3	0	1
3	StimDetailed	BAGLconnFrom3	2.57E-09	1
4	bhv	BAGLconnFrom3	0	3
4	FWD	BAGLconnFrom3	0	2
4	Stim	BAGLconnFrom3	0.002219036	1
4	StimDetailed	BAGLconnFrom3	0	1
5	bhv	BAGLconnFrom3	0	3
5	FWD	BAGLconnFrom3	0	2
5	Stim	BAGLconnFrom3	0	1
5	StimDetailed	BAGLconnFrom3	0	1
6	bhv	BAGLconnFrom3	0	3
6	FWD	BAGLconnFrom3	0	2
6	Stim	BAGLconnFrom3	0	2
6	StimDetailed	BAGLconnFrom3	0	1
7	bhv	BAGLconnFrom3	1.36E-05	3
7	FWD	BAGLconnFrom3	0.974016539	2
7	Stim	BAGLconnFrom3	8.16E-06	1
7	StimDetailed	BAGLconnFrom3	0.331185071	1
1	bhv	BAGLconnTo	0	1
1	FWD	BAGLconnTo	0	2
1	Stim	BAGLconnTo	3.61E-08	1
1	StimDetailed	BAGLconnTo	0.43877668	1
2	bhv	BAGLconnTo	0	3
2	FWD	BAGLconnTo	0	2
2	Stim	BAGLconnTo	0	2
2	StimDetailed	BAGLconnTo	0	1
3	bhv	BAGLconnTo	0	1
3	FWD	BAGLconnTo	0	1
3	Stim	BAGLconnTo	1.18E-13	2
3	StimDetailed	BAGLconnTo	0	2
4	bhv	BAGLconnTo	0.001282943	3
4	FWD	BAGLconnTo	0.001874833	2
4	Stim	BAGLconnTo	0.000111436	2
4	StimDetailed	BAGLconnTo	0.453219191	1
5	bhv	BAGLconnTo	0	3
5	FWD	BAGLconnTo	0	2
5	Stim	BAGLconnTo	0	1
5	StimDetailed	BAGLconnTo	0	1
6	bhv	BAGLconnTo	0	3
6	FWD	BAGLconnTo	0	2

6	Stim	BAGLconnTo	0	2
6	StimDetailed	BAGLconnTo	0	1
7	bhv	BAGLconnTo	0	3
7	FWD	BAGLconnTo	5.00E-08	2
7	Stim	BAGLconnTo	1.17E-12	1
7	StimDetailed	BAGLconnTo	0.414135974	1
1	bhv	BAGLconnTo3	0	1
1	FWD	BAGLconnTo3	0	1
1	Stim	BAGLconnTo3	0	2
1	StimDetailed	BAGLconnTo3	0	1
2	bhv	BAGLconnTo3	0	3
2	FWD	BAGLconnTo3	0	2
2	Stim	BAGLconnTo3	0	1
2	StimDetailed	BAGLconnTo3	0	1
3	bhv	BAGLconnTo3	0	1
3	FWD	BAGLconnTo3	0	1
3	Stim	BAGLconnTo3	0	2
3	StimDetailed	BAGLconnTo3	0	2
4	bhv	BAGLconnTo3	0	3
4	FWD	BAGLconnTo3	0	2
4	Stim	BAGLconnTo3	0	1
4	StimDetailed	BAGLconnTo3	0.000182064	1
5	bhv	BAGLconnTo3	0	3
5	FWD	BAGLconnTo3	0	2
5	Stim	BAGLconnTo3	0.000109209	1
5	StimDetailed	BAGLconnTo3	0.00015238	1
6	bhv	BAGLconnTo3	0	3
6	FWD	BAGLconnTo3	0	2
6	Stim	BAGLconnTo3	0	2
6	StimDetailed	BAGLconnTo3	5.94E-13	1
7	bhv	BAGLconnTo3	0	3
7	FWD	BAGLconnTo3	0	2
7	Stim	BAGLconnTo3	6.09E-07	1
7	StimDetailed	BAGLconnTo3	1.91E-07	1
1	bhv	BAGLyhat	0	3
1	FWD	BAGLyhat	0.082547706	2
1	StimD	BAGLyhat	0	1
1	Stim	BAGLyhat	1.80E-09	2
2	bhv	BAGLyhat	0	1
2	FWD	BAGLyhat	0	2
2	StimD	BAGLyhat	0.028008272	1
2	Stim	BAGLyhat	4.44E-16	2
3	bhv	BAGLyhat	0	3
3	FWD	BAGLyhat	0	2
3	StimD	BAGLyhat	0	1
3	Stim	BAGLyhat	0.000431215	2
4	bhv	BAGLyhat	0	3
4	FWD	BAGLyhat	0	2
4	StimD	BAGLyhat	0	1
4	Stim	BAGLyhat	0	2

5	bhv	BAGLyhat	0	1
5	FWD	BAGLyhat	5.00E-15	2
5	StimD	BAGLyhat	0	1
5	Stim	BAGLyhat	0	2
6	bhv	BAGLyhat	5.92E-13	3
6	FWD	BAGLyhat	0.000591953	2
6	StimD	BAGLyhat	0	1
6	Stim	BAGLyhat	0	2
7	bhv	BAGLyhat	0	1
7	FWD	BAGLyhat	1.82E-10	2
7	StimD	BAGLyhat	0	1
7	Stim	BAGLyhat	0	2
1	bhv	BAGLyhat3	3.59E-13	1
1	FWD	BAGLyhat3	4.95E-13	1
1	StimD	BAGLyhat3	0	2
1	Stim	BAGLyhat3	5.87E-14	2
2	bhv	BAGLyhat3	NaN	1
2	FWD	BAGLyhat3	NaN	1
2	StimD	BAGLyhat3	NaN	1
2	Stim	BAGLyhat3	NaN	1
3	bhv	BAGLyhat3	0	1
3	FWD	BAGLyhat3	0.387166233	1
3	StimD	BAGLyhat3	0	2
3	Stim	BAGLyhat3	4.11E-15	2
4	bhv	BAGLyhat3	0.000251191	3
4	FWD	BAGLyhat3	0.901473048	2
4	StimD	BAGLyhat3	0	2
4	Stim	BAGLyhat3	0	2
5	bhv	BAGLyhat3	0	4
5	FWD	BAGLyhat3	0.664427815	2
5	StimD	BAGLyhat3	0	2
5	Stim	BAGLyhat3	1.48E-09	2
6	bhv	BAGLyhat3	0	1
6	FWD	BAGLyhat3	0	1
6	StimD	BAGLyhat3	0	2
6	Stim	BAGLyhat3	0	2
7	bhv	BAGLyhat3	0	1
7	FWD	BAGLyhat3	8.51E-13	1
7	StimD	BAGLyhat3	0	2
7	Stim	BAGLyhat3	0	2
1	bhv	BAGRconnFrom	1.28E-05	3
1	FWD	BAGRconnFrom	0.014748755	2
1	Stim	BAGRconnFrom	1.98E-08	2
1	StimDetailed	BAGRconnFrom	5.41E-05	1
2	bhv	BAGRconnFrom	0.852212912	1
2	FWD	BAGRconnFrom	0.374550595	1
2	Stim	BAGRconnFrom	0.316950581	2
2	StimDetailed	BAGRconnFrom	0.563219514	1
3	bhv	BAGRconnFrom	0	1
3	FWD	BAGRconnFrom	0	1

3	Stim	BAGRconnFrom	0	1
3	StimDetailed	BAGRconnFrom	8.48E-08	1
4	bhv	BAGRconnFrom	2.81E-07	3
4	FWD	BAGRconnFrom	0.01013195	2
4	Stim	BAGRconnFrom	0.047476704	2
4	StimDetailed	BAGRconnFrom	0.017855089	1
5	bhv	BAGRconnFrom	0	3
5	FWD	BAGRconnFrom	0	2
5	Stim	BAGRconnFrom	0	1
5	StimDetailed	BAGRconnFrom	0	1
6	bhv	BAGRconnFrom	6.07E-08	3
6	FWD	BAGRconnFrom	8.14E-09	2
6	Stim	BAGRconnFrom	0.215820617	1
6	StimDetailed	BAGRconnFrom	7.15E-08	1
7	bhv	BAGRconnFrom	0	3
7	FWD	BAGRconnFrom	0.002875011	2
7	Stim	BAGRconnFrom	0.00376642	1
7	StimDetailed	BAGRconnFrom	0.180868357	1
1	bhv	BAGRconnFrom3	0	1
1	FWD	BAGRconnFrom3	0	1
1	Stim	BAGRconnFrom3	0	2
1	StimDetailed	BAGRconnFrom3	0	1
2	bhv	BAGRconnFrom3	0	1
2	FWD	BAGRconnFrom3	0	1
2	Stim	BAGRconnFrom3	0	2
2	StimDetailed	BAGRconnFrom3	0	1
3	bhv	BAGRconnFrom3	0	1
3	FWD	BAGRconnFrom3	0	1
3	Stim	BAGRconnFrom3	1.22E-15	1
3	StimDetailed	BAGRconnFrom3	1.10E-10	1
4	bhv	BAGRconnFrom3	0	3
4	FWD	BAGRconnFrom3	0	2
4	Stim	BAGRconnFrom3	0.001363628	1
4	StimDetailed	BAGRconnFrom3	0	1
5	bhv	BAGRconnFrom3	0	3
5	FWD	BAGRconnFrom3	0	2
5	Stim	BAGRconnFrom3	0	1
5	StimDetailed	BAGRconnFrom3	0	1
6	bhv	BAGRconnFrom3	0	3
6	FWD	BAGRconnFrom3	4.84E-11	2
6	Stim	BAGRconnFrom3	0	2
6	StimDetailed	BAGRconnFrom3	0	2
7	bhv	BAGRconnFrom3	2.36E-05	3
7	FWD	BAGRconnFrom3	0.400361255	2
7	Stim	BAGRconnFrom3	9.05E-05	1
7	StimDetailed	BAGRconnFrom3	0.084707144	1
1	bhv	BAGRconnTo	0	3
1	FWD	BAGRconnTo	0	2
1	Stim	BAGRconnTo	1.89E-10	1
1	StimDetailed	BAGRconnTo	0.385065329	1

2	bhv	BAGRconnTo	8.04E-14	1
2	FWD	BAGRconnTo	0.026228066	1
2	Stim	BAGRconnTo	0.00800951	2
2	StimDetailed	BAGRconnTo	0.125596464	1
3	bhv	BAGRconnTo	0	1
3	FWD	BAGRconnTo	7.85E-13	1
3	Stim	BAGRconnTo	0	2
3	StimDetailed	BAGRconnTo	0	2
4	bhv	BAGRconnTo	4.69E-14	3
4	FWD	BAGRconnTo	2.80E-14	2
4	Stim	BAGRconnTo	0.035427176	2
4	StimDetailed	BAGRconnTo	0.094578483	1
5	bhv	BAGRconnTo	0	3
5	FWD	BAGRconnTo	0	2
5	Stim	BAGRconnTo	0	1
5	StimDetailed	BAGRconnTo	0	1
6	bhv	BAGRconnTo	0	3
6	FWD	BAGRconnTo	0	2
6	Stim	BAGRconnTo	0	2
6	StimDetailed	BAGRconnTo	0	1
7	bhv	BAGRconnTo	0	3
7	FWD	BAGRconnTo	0	2
7	Stim	BAGRconnTo	0	2
7	StimDetailed	BAGRconnTo	2.59E-12	1
1	bhv	BAGRconnTo3	0	1
1	FWD	BAGRconnTo3	0	1
1	Stim	BAGRconnTo3	0	2
1	StimDetailed	BAGRconnTo3	0	1
2	bhv	BAGRconnTo3	0	1
2	FWD	BAGRconnTo3	0	2
2	Stim	BAGRconnTo3	0	2
2	StimDetailed	BAGRconnTo3	0	1
3	bhv	BAGRconnTo3	0	1
3	FWD	BAGRconnTo3	0	1
3	Stim	BAGRconnTo3	0	2
3	StimDetailed	BAGRconnTo3	0	2
4	bhv	BAGRconnTo3	0	3
4	FWD	BAGRconnTo3	0	2
4	Stim	BAGRconnTo3	0	1
4	StimDetailed	BAGRconnTo3	3.43E-06	1
5	bhv	BAGRconnTo3	0	3
5	FWD	BAGRconnTo3	0	2
5	Stim	BAGRconnTo3	6.68E-07	1
5	StimDetailed	BAGRconnTo3	0.004446872	1
6	bhv	BAGRconnTo3	0	3
6	FWD	BAGRconnTo3	0	2
6	Stim	BAGRconnTo3	0	2
6	StimDetailed	BAGRconnTo3	1.11E-16	1
7	bhv	BAGRconnTo3	0	3
7	FWD	BAGRconnTo3	0	2

7	Stim	BAGRconnTo3	3.09E-07	1
7	StimDetailed	BAGRconnTo3	2.18E-05	1
1	bhv	BAGRyhat	0	1
1	FWD	BAGRyhat	2.35E-05	2
1	StimD	BAGRyhat	0	1
1	Stim	BAGRyhat	6.00E-07	2
2	bhv	BAGRyhat	0	3
2	FWD	BAGRyhat	0	2
2	StimD	BAGRyhat	0.433150492	1
2	Stim	BAGRyhat	0	1
3	bhv	BAGRyhat	0	3
3	FWD	BAGRyhat	0	2
3	StimD	BAGRyhat	0	1
3	Stim	BAGRyhat	0.020047127	2
4	bhv	BAGRyhat	0	3
4	FWD	BAGRyhat	0	2
4	StimD	BAGRyhat	0	1
4	Stim	BAGRyhat	0	2
5	bhv	BAGRyhat	3.49E-13	3
5	FWD	BAGRyhat	0.094265537	2
5	StimD	BAGRyhat	0	1
5	Stim	BAGRyhat	0	2
6	bhv	BAGRyhat	0	3
6	FWD	BAGRyhat	0.000109988	2
6	StimD	BAGRyhat	0	1
6	Stim	BAGRyhat	0	2
7	bhv	BAGRyhat	1.47E-09	3
7	FWD	BAGRyhat	0.271370652	2
7	StimD	BAGRyhat	0	1
7	Stim	BAGRyhat	0	2
1	bhv	BAGRyhat3	1.65E-13	1
1	FWD	BAGRyhat3	2.05E-13	1
1	StimD	BAGRyhat3	0	2
1	Stim	BAGRyhat3	3.44E-14	2
2	bhv	BAGRyhat3	NaN	1
2	FWD	BAGRyhat3	NaN	1
2	StimD	BAGRyhat3	NaN	1
2	Stim	BAGRyhat3	NaN	1
3	bhv	BAGRyhat3	0	1
3	FWD	BAGRyhat3	0.550846632	1
3	StimD	BAGRyhat3	0	2
3	Stim	BAGRyhat3	6.03E-14	2
4	bhv	BAGRyhat3	0.000115954	3
4	FWD	BAGRyhat3	0.681885281	2
4	StimD	BAGRyhat3	0	2
4	Stim	BAGRyhat3	0	2
5	bhv	BAGRyhat3	0	4
5	FWD	BAGRyhat3	0.352915814	2
5	StimD	BAGRyhat3	0	2
5	Stim	BAGRyhat3	1.77E-10	2

6	bhv	BAGRyhat3	0	1
6	FWD	BAGRyhat3	0	1
6	StimD	BAGRyhat3	0	2
6	Stim	BAGRyhat3	0	2
7	bhv	BAGRyhat3	0	1
7	FWD	BAGRyhat3	3.83E-13	1
7	StimD	BAGRyhat3	0	2
7	Stim	BAGRyhat3	0	2
1	bhv	RMEDconnFrom	0	3
1	FWD	RMEDconnFrom	0	2
1	Stim	RMEDconnFrom	0	1
1	StimDetailed	RMEDconnFrom	0.002563748	1
2	bhv	RMEDconnFrom	0.852212912	1
2	FWD	RMEDconnFrom	0.374550595	1
2	Stim	RMEDconnFrom	0.316950581	2
2	StimDetailed	RMEDconnFrom	0.563219514	1
3	bhv	RMEDconnFrom	0	1
3	FWD	RMEDconnFrom	0	1
3	Stim	RMEDconnFrom	2.45E-13	1
3	StimDetailed	RMEDconnFrom	0.218018517	1
4	bhv	RMEDconnFrom	0.007016026	3
4	FWD	RMEDconnFrom	0.521763493	2
4	Stim	RMEDconnFrom	0.317190572	2
4	StimDetailed	RMEDconnFrom	0.563348559	1
5	bhv	RMEDconnFrom	0	3
5	FWD	RMEDconnFrom	0	2
5	Stim	RMEDconnFrom	0	1
5	StimDetailed	RMEDconnFrom	0	1
6	bhv	RMEDconnFrom	4.90E-12	3
6	FWD	RMEDconnFrom	0.001121497	2
6	Stim	RMEDconnFrom	0	2
6	StimDetailed	RMEDconnFrom	0	1
7	bhv	RMEDconnFrom	1.09E-07	3
7	FWD	RMEDconnFrom	0.017040683	2
7	Stim	RMEDconnFrom	1.04E-11	1
7	StimDetailed	RMEDconnFrom	0.920508447	1
1	bhv	RMEDconnFrom3	0	3
1	FWD	RMEDconnFrom3	0	2
1	Stim	RMEDconnFrom3	0	1
1	StimDetailed	RMEDconnFrom3	0	1
2	bhv	RMEDconnFrom3	0	3
2	FWD	RMEDconnFrom3	0	2
2	Stim	RMEDconnFrom3	0.120316069	2
2	StimDetailed	RMEDconnFrom3	7.08E-10	1
3	bhv	RMEDconnFrom3	0	1
3	FWD	RMEDconnFrom3	0	1
3	Stim	RMEDconnFrom3	0	2
3	StimDetailed	RMEDconnFrom3	3.09E-11	1
4	bhv	RMEDconnFrom3	0	1
4	FWD	RMEDconnFrom3	0	2

4	Stim	RMEDconnFrom3	1.94E-08	2
4	StimDetailed	RMEDconnFrom3	5.21E-14	1
5	bhv	RMEDconnFrom3	0	3
5	FWD	RMEDconnFrom3	0	2
5	Stim	RMEDconnFrom3	0	1
5	StimDetailed	RMEDconnFrom3	0	1
6	bhv	RMEDconnFrom3	7.27E-13	3
6	FWD	RMEDconnFrom3	0.043686063	2
6	Stim	RMEDconnFrom3	0	2
6	StimDetailed	RMEDconnFrom3	0	1
7	bhv	RMEDconnFrom3	0	3
7	FWD	RMEDconnFrom3	0	2
7	Stim	RMEDconnFrom3	0	1
7	StimDetailed	RMEDconnFrom3	2.12E-14	1
1	bhv	RMEDconnTo	0.153422366	3
1	FWD	RMEDconnTo	0.455954039	2
1	Stim	RMEDconnTo	0.317200396	2
1	StimDetailed	RMEDconnTo	0.563377578	1
2	bhv	RMEDconnTo	0	3
2	FWD	RMEDconnTo	0	2
2	Stim	RMEDconnTo	0	2
2	StimDetailed	RMEDconnTo	0	1
3	bhv	RMEDconnTo	0	1
3	FWD	RMEDconnTo	0	1
3	Stim	RMEDconnTo	0.107255177	2
3	StimDetailed	RMEDconnTo	0.00955524	1
4	bhv	RMEDconnTo	4.11E-07	3
4	FWD	RMEDconnTo	3.02E-07	2
4	Stim	RMEDconnTo	0.020235642	2
4	StimDetailed	RMEDconnTo	0.053461171	1
5	bhv	RMEDconnTo	0	3
5	FWD	RMEDconnTo	0	2
5	Stim	RMEDconnTo	0	1
5	StimDetailed	RMEDconnTo	0	1
6	bhv	RMEDconnTo	1.17E-11	3
6	FWD	RMEDconnTo	0.286958465	2
6	Stim	RMEDconnTo	0	2
6	StimDetailed	RMEDconnTo	0	1
7	bhv	RMEDconnTo	0	3
7	FWD	RMEDconnTo	0	2
7	Stim	RMEDconnTo	0.003467701	2
7	StimDetailed	RMEDconnTo	0.836753348	1
1	bhv	RMEDconnTo3	0	1
1	FWD	RMEDconnTo3	0	2
1	Stim	RMEDconnTo3	6.08E-09	1
1	StimDetailed	RMEDconnTo3	0.302351635	1
2	bhv	RMEDconnTo3	0	3
2	FWD	RMEDconnTo3	0	2
2	Stim	RMEDconnTo3	0.169794192	2
2	StimDetailed	RMEDconnTo3	7.23E-10	1

3	bhv	RMEDconnTo3	9.20E-12	1
3	FWD	RMEDconnTo3	0.004645027	1
3	Stim	RMEDconnTo3	4.40E-10	1
3	StimDetailed	RMEDconnTo3	3.02E-05	1
4	bhv	RMEDconnTo3	0	1
4	FWD	RMEDconnTo3	0	2
4	Stim	RMEDconnTo3	0	2
4	StimDetailed	RMEDconnTo3	2.46E-08	1
5	bhv	RMEDconnTo3	0	3
5	FWD	RMEDconnTo3	0	2
5	Stim	RMEDconnTo3	0	1
5	StimDetailed	RMEDconnTo3	0	1
6	bhv	RMEDconnTo3	4.44E-15	3
6	FWD	RMEDconnTo3	0.089729144	2
6	Stim	RMEDconnTo3	0	2
6	StimDetailed	RMEDconnTo3	0	1
7	bhv	RMEDconnTo3	0	3
7	FWD	RMEDconnTo3	0	2
7	Stim	RMEDconnTo3	0.004124427	2
7	StimDetailed	RMEDconnTo3	0.009771305	1
1	bhv	RMEDyhat	0	1
1	FWD	RMEDyhat	0	1
1	StimD	RMEDyhat	1.57E-14	1
1	Stim	RMEDyhat	0	2
2	bhv	RMEDyhat	0	1
2	FWD	RMEDyhat	0	1
2	StimD	RMEDyhat	8.84E-10	1
2	Stim	RMEDyhat	0.462476328	2
3	bhv	RMEDyhat	0	1
3	FWD	RMEDyhat	0	1
3	StimD	RMEDyhat	0.720606572	1
3	Stim	RMEDyhat	3.24E-11	1
4	bhv	RMEDyhat	0	1
4	FWD	RMEDyhat	0	1
4	StimD	RMEDyhat	0	1
4	Stim	RMEDyhat	5.96E-11	1
5	bhv	RMEDyhat	0	1
5	FWD	RMEDyhat	0	1
5	StimD	RMEDyhat	1.67E-13	1
5	Stim	RMEDyhat	0	2
6	bhv	RMEDyhat	0	1
6	FWD	RMEDyhat	0	1
6	StimD	RMEDyhat	1.97E-09	1
6	Stim	RMEDyhat	0	2
7	bhv	RMEDyhat	0	1
7	FWD	RMEDyhat	0	1
7	StimD	RMEDyhat	0.002328889	1
7	Stim	RMEDyhat	0.000561525	1
1	bhv	RMEDyhat3	6.11E-08	4
1	FWD	RMEDyhat3	0.093215461	2

1	StimD	RMEDyhat3	0.030122615	1
1	Stim	RMEDyhat3	0.000174292	1
2	bhv	RMEDyhat3	NaN	1
2	FWD	RMEDyhat3	NaN	1
2	StimD	RMEDyhat3	NaN	1
2	Stim	RMEDyhat3	NaN	1
3	bhv	RMEDyhat3	0.692525385	1
3	FWD	RMEDyhat3	0.227611112	1
3	StimD	RMEDyhat3	0.411452983	1
3	Stim	RMEDyhat3	0.999486166	1
4	bhv	RMEDyhat3	0	1
4	FWD	RMEDyhat3	0	1
4	StimD	RMEDyhat3	0.000269154	1
4	Stim	RMEDyhat3	2.86E-10	1
5	bhv	RMEDyhat3	0	4
5	FWD	RMEDyhat3	0.001032524	2
5	StimD	RMEDyhat3	1.44E-15	2
5	Stim	RMEDyhat3	4.17E-06	2
6	bhv	RMEDyhat3	NaN	1
6	FWD	RMEDyhat3	NaN	1
6	StimD	RMEDyhat3	NaN	1
6	Stim	RMEDyhat3	NaN	1
7	bhv	RMEDyhat3	NaN	1
7	FWD	RMEDyhat3	NaN	1
7	StimD	RMEDyhat3	NaN	1
7	Stim	RMEDyhat3	NaN	1
1	bhv	stimTimes	0	1
1	FWD	stimTimes	0	2
2	bhv	stimTimes	0.005427256	1
2	FWD	stimTimes	0.144226273	1
3	bhv	stimTimes	0	1
3	FWD	stimTimes	0	1
4	bhv	stimTimes	0.002227528	3
4	FWD	stimTimes	0.000719659	2
5	bhv	stimTimes	0	1
5	FWD	stimTimes	0	1
6	bhv	stimTimes	1.55E-13	3
6	FWD	stimTimes	6.57E-13	2
7	bhv	stimTimes	6.01E-10	3
7	FWD	stimTimes	1.63E-11	2
1	bhv	stimTimesDetailed	0	1
1	FWD	stimTimesDetailed	1.11E-16	1
2	bhv	stimTimesDetailed	5.05E-08	1
2	FWD	stimTimesDetailed	4.49E-05	2
3	bhv	stimTimesDetailed	7.11E-14	1
3	FWD	stimTimesDetailed	9.01E-10	1
4	bhv	stimTimesDetailed	2.38E-14	3
4	FWD	stimTimesDetailed	1.55E-14	2
5	bhv	stimTimesDetailed	3.97E-07	1
5	FWD	stimTimesDetailed	5.63E-06	2

6	bhv	stimTimesDetailed	3.49E-05	3
6	FWD	stimTimesDetailed	2.14E-05	2
7	bhv	stimTimesDetailed	3.38E-09	3
7	FWD	stimTimesDetailed	1.89E-07	2

Table 4: χ^2 **tests for BAG and RMED activity and connectivity (inactive vs. active above a threshold), behavior, and oxygen stimulation levels**.

6.5 ANOVA and MANOVA tests

In order to test effects of categorical factors such as oxygen stimulation settings and behavior states on individual neuron activity and connectivity, we conducted ANOVA and MANOVA tests (with Roy's Largest Root) (ANOVA; MANOVA) for each Stim worm per-worm model (p-values in Table 5). All of the tests with connectivity to and from each neuron were found to be significant for Behavior (1-4), Stimulation (0 or 1, i.e., 21% oxygen first half vs. alternating oxygen levels second half), and interaction between the levels of Behavior and Stimulation. Most of the activity tests were also significant to varying degrees ($\alpha = 1 * 10^{-4}$ to 0.05, depending on the correction for multiple tests).

Neuron	Worm	Dep. Var.	Behavior p	Stim (1st half/2nd) p	Behavior:Stim p	Adj R^2
AVFR	1	connFrom	0.00E+00	6.15E-76	1.30E-183	
AVFR	2	connFrom	0.00E+00	0.00E+00	0.00E+00	
AVFR	3	connFrom	0.00E+00	6.41E-142	0.00E+00	
AVFR	4	connFrom	0.00E+00	3.79E-216	0.00E+00	
AVFR	5	connFrom	0.00E+00	0.00E+00	0.00E+00	
AVFR	6	connFrom	0.00E+00	2.06E-274	0.00E+00	
AVFR	7	connFrom	0	4.44E-265	0	
BAGL	1	connFrom	0.00E+00	6.15E-76	6.58E-203	
BAGL	2	connFrom	0.00E+00	0.00E+00	0.00E+00	
BAGL	3	connFrom	0.00E+00	3.35E-178	0.00E+00	
BAGL	4	connFrom	0.00E+00	2.25E-244	0.00E+00	
BAGL	5	connFrom	0.00E+00	0.00E+00	0.00E+00	
BAGL	6	connFrom	0.00E+00	0.00E+00	0.00E+00	
BAGL	7	connFrom	0	4.44E-265	0	
BAGR	1	connFrom	0.00E+00	6.15E-76	1.30E-183	
BAGR	2	connFrom	0.00E+00	0.00E+00	0.00E+00	
BAGR	3	connFrom	0.00E+00	1.43E-192	6.05E-236	
BAGR	4	connFrom	0.00E+00	0.00E+00	0.00E+00	
BAGR	5	connFrom	0.00E+00	0.00E+00	0.00E+00	
BAGR	6	connFrom	0.00E+00	0.00E+00	0.00E+00	
BAGR	7	connFrom	0	0	0	
RIGL	1	connFrom				
RIGL	2	connFrom	0.00E+00	0.00E+00	0.00E+00	
RIGL	3	connFrom	0.00E+00	6.41E-142	6.05E-236	
RIGL	4	connFrom	0.00E+00	0.00E+00	0.00E+00	
RIGL	5	connFrom				
RIGL	6	connFrom	0.00E+00	2.06E-274	0.00E+00	
RIGL	7	connFrom				
RIS	1	connFrom	0.00E+00	6.15E-76	0.00E+00	
RIS	2	connFrom	0.00E+00	0.00E+00	0.00E+00	
RIS	3	connFrom	0.00E+00	6.41E-142	0.00E+00	
RIS	4	connFrom	0.00E+00	0.00E+00	0.00E+00	

RIS	5	connFrom	0.00E+00	0.00E+00	0.00E+00
RIS	6	connFrom	0.00E+00	2.06E-274	0.00E+00
RIS	7	connFrom			
RMED	1	connFrom	0.00E+00	6.15E-76	1.30E-183
RMED	2	connFrom	0.00E+00	0.00E+00	0.00E+00
RMED	3	connFrom	0.00E+00	4.88E-203	6.05E-236
RMED	4	connFrom	0.00E+00	3.79E-216	0.00E+00
RMED	5	connFrom	0.00E+00	0.00E+00	0.00E+00
RMED	6	connFrom	0.00E+00	0.00E+00	0.00E+00
RMED	7	connFrom	0	1.68E-295	2.26E-296
SABD	1	connFrom	0.00E+00	6.15E-76	1.30E-183
SABD	2	connFrom			
SABD	3	connFrom			
SABD	4	connFrom			
SABD	5	connFrom			
SABD	6	connFrom			
SABD	7	connFrom			
AVFR	1	connTo	0.00E+00	6.15E-76	0.00E+00
AVFR	2	connTo	0.00E+00	0.00E+00	0.00E+00
AVFR	3	connTo	0.00E+00	6.41E-142	6.05E-236
AVFR	4	connTo	0.00E+00	3.79E-216	0.00E+00
AVFR	5	connTo	0.00E+00	0.00E+00	0.00E+00
AVFR	6	connTo	0.00E+00	2.06E-274	0.00E+00
AVFR	7	connTo	0	4.44E-265	0
BAGL	1	connTo	0.00E+00	6.15E-76	0.00E+00
BAGL	2	connTo	0.00E+00	0.00E+00	0.00E+00
BAGL	3	connTo	0.00E+00	6.41E-142	0.00E+00
BAGL	4	connTo	0.00E+00	0.00E+00	0.00E+00
BAGL	5	connTo	0.00E+00	0.00E+00	0.00E+00
BAGL	6	connTo	0.00E+00	0.00E+00	0.00E+00
BAGL	7	connTo	0	9.17E-268	0.00E+00
BAGR	1	connTo	0.00E+00	6.15E-76	0.00E+00
BAGR	2	connTo	0.00E+00	0.00E+00	0.00E+00
BAGR	3	connTo	0.00E+00	6.41E-142	6.05E-236
BAGR	4	connTo	0.00E+00	0.00E+00	0.00E+00
BAGR	5	connTo	0.00E+00	0.00E+00	0.00E+00
BAGR	6	connTo	0.00E+00	0.00E+00	0.00E+00
BAGR	7	connTo	0	4.44E-265	2.26E-296
RIGL	1	connTo			
RIGL	2	connTo	0.00E+00	0.00E+00	0.00E+00
RIGL	3	connTo	0.00E+00	6.41E-142	6.05E-236
RIGL	4	connTo	0.00E+00	3.79E-216	0.00E+00
RIGL	5	connTo			
RIGL	6	connTo	0.00E+00	2.06E-274	0.00E+00
RIGL	7	connTo			
RIS	1	connTo	0.00E+00	6.15E-76	7.47E-268
RIS	2	connTo	0.00E+00	0.00E+00	0.00E+00
RIS	3	connTo	0.00E+00	6.41E-142	6.05E-236
RIS	4	connTo	0.00E+00	4.94E-289	2.59E-301
RIS	5	connTo	0.00E+00	0.00E+00	0.00E+00

RIS	6	connTo	0.00E+00	2.61E-276	0.00E+00	
RIS	7	connTo				
RMED	1	connTo	0.00E+00	5.96E-150	1.30E-183	
RMED	2	connTo	0.00E+00	0.00E+00	0.00E+00	
RMED	3	connTo	0.00E+00	6.41E-142	6.05E-236	
RMED	4	connTo	0.00E+00	0.00E+00	9.92E-273	
RMED	5	connTo	0.00E+00	0.00E+00	0.00E+00	
RMED	6	connTo	0.00E+00	2.06E-274	0.00E+00	
RMED	7	connTo	0	4.44E-265	0	
SABD	1	connTo	0.00E+00	6.15E-76	0.00E+00	
SABD	2	connTo				
SABD	3	connTo				
SABD	4	connTo				
SABD	5	connTo				
SABD	6	connTo				
SABD	7	connTo				
AVFR	1	yhat	2.53E-121	5.85E-51	4.35E-10	0.27271
AVFR	2	yhat	2.31E-276	1.53E-26	2.16E-54	0.50246
AVFR	3	yhat	1.03E-192	1.95E-45	1.45E-08	0.39142
AVFR	4	yhat	1.95E-307	6.65E-151	2.24E-14	0.6152
AVFR	5	yhat	2.07E-130	0.22397	1.13E-105	0.3189
AVFR	6	yhat	7.53E-176	1.12E-07	7.11E-19	0.3633
AVFR	7	yhat	1.06E-61	0.76898	1.01E-14	0.16516
BAGL	1	yhat	1.41E-12	1.47E-05	2.78E-10	0.070177
BAGL	2	yhat	1.88E-149	1.92E-99	1.03E-94	0.45291
BAGL	3	yhat	1.40E-65	1.25E-53	5.24E-56	0.2643
BAGL	4	yhat	4.38E-26	1.03E-54	5.74E-22	0.19886
BAGL	5	yhat	8.21E-120	8.47E-103	1.19E-102	0.38648
BAGL	6	yhat	1.25E-54	2.97E-50	5.17E-32	0.2855
BAGL	7	yhat	1.98E-85	2.59E-68	3.99E-68	0.39631
BAGR	1	yhat	1.74E-14	6.22E-06	1.44E-11	0.078149
BAGR	2	yhat	2.02E-207	0.13666	3.22E-83	0.45733
BAGR	3	yhat	1.86E-68	4.16E-41	6.05E-59	0.24996
BAGR	4	yhat	2.20E-47	1.61E-52	6.28E-21	0.22644
BAGR	5	yhat	2.32E-123	7.95E-101	2.21E-106	0.3766
BAGR	6	yhat	8.18E-31	7.11E-43	1.52E-32	0.22165
BAGR	7	yhat	1.90E-59	2.97E-63	7.89E-66	0.36191
RIGL	1	yhat				
RIGL	2	yhat	1.96E-157	8.53E-37	5.23E-79	0.48436
RIGL	3	yhat	3.63E-203	3.30E-28	0.181	0.3797
RIGL	4	yhat	2.21E-86	0.11906	2.66E-09	0.18101
RIGL	5	yhat				
RIGL	6	yhat	1.11E-166	0.29801	9.56E-49	0.40334
RIGL	7	yhat				
RIS	1	yhat	3.71E-167	0.31206	3.68E-46	0.3906
RIS	2	yhat	4.25E-117	1.85E-62	4.81E-103	0.54036
RIS	3	yhat	0.00E+00	5.85E-13	1.90E-09	0.58904
RIS	4	yhat	0.00E+00	4.79E-47	5.53E-151	0.68606
RIS	5	yhat	0.00E+00	1.80E-161	2.40E-267	0.79257
RIS	6	yhat	4.25E-164	1.01E-40	5.55E-48	0.48265

RIS	7	yhat				
RMED	1	yhat	1.56E-278	0.006158	5.60E-14	0.47583
RMED	2	yhat	0.00E+00	1.06E-13	8.10E-11	0.5958
RMED	3	yhat	3.12E-248	7.57E-36	0.017463	0.43344
RMED	4	yhat	0.00E+00	3.76E-124	3.28E-94	0.79162
RMED	5	yhat	0.00E+00	4.41E-13	9.93E-131	0.6654
RMED	6	yhat	0.00E+00	5.14E-08	1.16E-06	0.79017
RMED	7	yhat	0.00E+00	6.97E-31	3.21E-16	0.85821
SABD	1	yhat	0.00E+00	0.001283	2.18E-15	0.54474
SABD	2	yhat				
SABD	3	yhat				
SABD	4	yhat				
SABD	5	yhat				
SABD	6	yhat				
SABD	7	yhat				

Table 5: **ANOVA and MANOVA tests for AVFR, BAGL, BAGR, RIGL, RIS, RMED, and SABD activity and connectivity vs. behavior and oxygen stimulation factor levels**.

6.6 RMED dynamic connectivity tally

Table 6 is a tally of strong connectivity with or activity in BAGR and/or BAGL across the worms' dynamic connectivity maps for each DO.

subset	per-worm DOs	worms	aligned DOs	worms
Stim FWD	22/31	6/7	35/46	7/7
Stim REVSUS	4/36	3/7	8/54	3/7
Stim only 1st half	0/3	0/7	1/6	1/7
Stim mostly 1st half	3/11	2/7	4/8	2/7
Stim mostly 2nd half	4/8	2/7	6/9	3/7
Stim only 2nd half	8/9	4/7	12/20	7/7
Stim sign flip between halves	2/3	2/7	0/1	0/7
NoStim FWD	17/21	5/5		
NoStim SLOW	20/27	5/5		
NoStim REVSUS	3/23	3/5		

Table 6: **Tally of RMED presence in dynamic connectivity maps across conditions.**

References

Z. Altun. Wormatlas individual neurons, 2014. URL https://www.wormatlas.org/neurons/Individual%20Neurons/Neuronframeset.html.

ANOVA. Analysis of variance (anova) results - matlab. URL https://www.mathworks.com/help/stats/anova.html.

Evan L. Ardiel and Catharine H. Rankin. An elegant mind: Learning and memory in caenorhabditis elegans, 4 2010. ISSN 10720502.

Adam A. Atanas, Jungsoo Kim, Ziyu Wang, Eric Bueno, McCoy Becker, Di Kang, Jungyeon Park, Talya S. Kramer, Flossie K. Wan, Saba Baskoylu, Ugur Dag, Elpiniki Kalogeropoulou, Matthew A. Gomes, Cassi Estrem, Netta Cohen, Vikash K. Mansinghka, and Steven W. Flavell. Brain-wide representations of behavior spanning multiple timescales and states in c. elegans. *Cell*, 8 2023. ISSN 00928674. doi: 10.1016/j.cell.2023.07.035. URL https://linkinghub.elsevier.com/retrieve/pii/S0092867423008504.

Atlas. Neuronal wiring. URL https://www.wormatlas.org/neuronalwiring.html#NeuronalconnectivityII.

Peder Axensten. chi2test, 2007. URL https://www.mathworks.com/matlabcentral/fileexchange/16177-chi2test.

Isabel Beets, Sven Zels, Elke Vandewyer, Jonas Demeulemeester, Jelle Caers, Esra Baytemur, William R Schafer, Petra E Vértes, Olivier Mirabeau, and Liliane Schoofs. System-wide mapping of neuropeptide-gpcr interactions in c. elegans. *bioRxiv*, 2022. doi: 10.1101/2022.10.30.514428. URL https://doi.org/10.1101/2022.10.30.514428.

Bingni W. Brunton, Lise A. Johnson, Jeffrey G. Ojemann, and J. Nathan Kutz. Extracting spatial-temporal coherent patterns in large-scale neural recordings using dynamic mode decomposition. *Journal of Neuroscience Methods*, 258:1–15, 1 2016. ISSN 1872678X. doi: 10.1016/j.jneumeth.2015.10.010.

Steven J. Cook, Travis A. Jarrell, Christopher A. Brittin, Yi Wang, Adam E. Bloniarz, Maksim A. Yakovlev, Ken C.Q. Nguyen, Leo T.H. Tang, Emily A. Bayer, Janet S. Duerr, Hannes E. Bülow, Oliver Hobert, David H. Hall, and Scott W. Emmons. Whole-animal connectomes of both caenorhabditis elegans sexes. *Nature*, 571:63–71, 7 2019. ISSN 14764687. doi: 10.1038/s41586-019-1352-7.

Antonio C. Costa, Tosif Ahamed, and Greg J. Stephens. Adaptive, locally linear models of complex dynamics. *Proceedings of the National Academy of Sciences of the United States of America*, 116:1501–1510, 1 2019. ISSN 10916490. doi: 10.1073/pnas.1813476116.

Steven W. Flavell and Andrew Gordus. Dynamic functional connectivity in the static connectome of caenorhabditis elegans, 4 2022. ISSN 18736882.

Eleni Gourgou, Kavya Adiga, Anne Goettemoeller, Chieh Chen, and Ao Lin Hsu. Caenorhabditis elegans learning in a structured maze is a multisensory behavior. *iScience*, 24, 4 2021. ISSN 25890042. doi: 10.1016/j.isci.2021.102284.

Kelsey M. Hallinen, Ross Dempsey, Monika Scholz, Xinwei Yu, Ashley Linder, Francesco Randi, Anuj Sharma, Joshua W. Shaevitz, and Andrew M. Leifer. Decoding locomotion from population neural activity in moving c. elegans. *eLife*, 10, 7 2021. ISSN 2050084X. doi: 10.7554/eLife.66135.

Jingyuan Jiang, Yifan Su, Ruilin Zhang, Haiwen Li, Louis Tao, and Qiang Liu. C. elegans enteric motor neurons fire synchronized action potentials underlying the defecation motor program. *Nature Communications*, 13, 12 2022. ISSN 20411723. doi: 10.1038/s41467-022-30452-y.

Saul Kato, Harris S. Kaplan, Tina Schrödel, Susanne Skora, Theodore H. Lindsay, Eviatar Yemini, Shawn Lockery, and Manuel Zimmer. Global Brain Dynamics Embed the Motor Command Sequence of Caenorhabditis elegans. *Cell*, 163(3):656–669, 2015. ISSN 10974172. doi: 10.1016/j.cell.2015.09.034.

Dennis H. Kim and Steven W. Flavell. Host-microbe interactions and the behavior of caenorhabditis elegans, 2020. ISSN 15635260.

Scott Linderman, Benjamin Antin, David Zoltowski, and Joshua Glaser. SSM: Bayesian Learning and Inference for State Space Models (version 0.0.1, 10 2020. URL `https://github.com/lindermanlab/ssm`.

Scott W. Linderman, Annika L. A. Nichols, David M. Blei, Manuel Zimmer, and Liam Paninski. Hierarchical recurrent state space models reveal discrete and continuous dynamics of neural activity in C. elegans. *bioRxiv*, page 621540, 2019. doi: 10.1101/621540. URL `https://www.biorxiv.org/content/10.1101/621540v1.abstract?%3Fcollection=`.

Theodore H. Lindsay, Tod R. Thiele, and Shawn R. Lockery. Optogenetic analysis of synaptic transmission in the central nervous system of the nematode caenorhabditis elegans. *Nature Communications*, 2, 2011. ISSN 20411723. doi: 10.1038/ncomms1304.

MANOVA. Multivariate analysis of variance (anova) results - matlab. URL `https://www.mathworks.com/help/stats/anova.html`.

Noga Mudrik, Yenho Chen, Eva Yezerets, Christopher J Rozell, and Adam S Charles. Decomposed linear dynamical systems (dlds) for learning the latent components of neural dynamics. *Journal of Machine Learning Research*, 25(59):1–44, 2024.

Annika L.A. Nichols, Tomáš Eichler, Richard Latham, and Manuel Zimmer. A global brain state underlies c. elegans sleep behavior. *Science*, 356:1247–1256, 2017. ISSN 10959203. doi: 10.1126/science.aam6851.

Aelon Rahmani and Yee Lian Chew. Investigating the molecular mechanisms of learning and memory using caenorhabditis elegans, 11 2021. ISSN 14714159.

Francesco Randi and Andrew M. Leifer. Measuring and modeling whole-brain neural dynamics in caenorhabditis elegans. *Current Opinion in Neurobiology*, 65:167–175, 12 2020. ISSN 18736882. doi: 10.1016/j.conb.2020.11.001.

Francesco Randi, Anuj K. Sharma, Sophie Dvali, and Andrew M. Leifer. Neural signal propagation atlas of caenorhabditis elegans. *Nature*, 623:406–414, 11 2023. ISSN 14764687. doi: 10.1038/s41586-023-06683-4.

Catharine H Rankin and Brett S Broster. Factors affecting habituation and recovery from habituation in the nematode caenorhabditis elegans, 1992.

Catherine H Rankin, Christine D O Beck, Catherine M Chiba, and C H Rankin. Caenorhabditis elegans: a new model system for the study of learning and memory, 1990.

Julia Riedl, Charles Fieseler, and Manuel Zimmer. Tyraminergic corollary discharge filters reafferent perception in a chemosensory neuron. *Current Biology*, 32:3048–3058.e6, 7 2022. ISSN 18790445. doi: 10.1016/j.cub.2022.05.051.

J. K. Rose and C. H. Rankin. Analyses of habituation in caenorhabditis elegans, 2001. ISSN 10720502.

Yu Shen, Quan Wen, He Liu, Connie Zhong, Yuqi Qin, Gareth Harris, Taizo Kawano, Min Wu, Tianqi Xu, Aravinthan DT Samuel, and Yun Zhang. An extrasynaptic gabaergic signal modulates a pattern of forward movement in caenorhabditis elegans. 2016. doi: 10.7554/eLife.14197.001.

Geneva M. Stein and Coleen T. Murphy. C. elegans positive olfactory associative memory is a molecularly conserved behavioral paradigm. *Neurobiology of Learning and Memory*, 115:86–94, 11 2014. ISSN 10959564. doi: 10.1016/j.nlm.2014.07.011.

Shay Stern, Christoph Kirst, and Cornelia I. Bargmann. Neuromodulatory control of long-term behavioral patterns and individuality across development. *Cell*, 171:1649–1662.e10, 12 2017. ISSN 10974172. doi: 10.1016/j.cell.2017.10.041.

Kerem Uzel, Saul Kato, and Manuel Zimmer. A set of hub neurons and non-local connectivity features support global brain dynamics in c. elegans. *Current Biology*, 32:3443–3459.e8, 8 2022. doi: 10.1016/J.CUB.2022.06.039.

Han Wang, Kelly Girskis, Tom Janssen, Jason P. Chan, Krishnakali Dasgupta, James A. Knowles, Liliane Schoofs, and Derek Sieburth. Neuropeptide secreted from a pacemaker activates neurons to control a rhythmic behavior. *Current Biology*, 23:746–754, 5 2013. ISSN 09609822. doi: 10.1016/j.cub.2013.03.049.

J. G. White, E. Southgate, J. N. Thomson, and S. Brenner. The structure of the nervous system of the nematode caenorhabditis elegans. *Philosophical Transactions of the Royal Society of London*, 314, 1986. URL `https://royalsocietypublishing.org/`.

Daniel Witvliet, Ben Mulcahy, James K. Mitchell, Yaron Meirovitch, Daniel R. Berger, Yuelong Wu, Yufang Liu, Wan Xian Koh, Rajeev Parvathala, Douglas Holmyard, Richard L. Schalek, Nir Shavit, Andrew D. Chisholm, Jeff W. Lichtman, Aravinthan D.T. Samuel, and Mei Zhen. Connectomes across development reveal principles of brain maturation. *Nature*, 596:257–261, 8 2021. ISSN 14764687. doi: 10.1038/s41586-021-03778-8.

Manuel Zimmer. Kato2015 whole brain imaging data, January 2021. URL `osf.io/2395t`.

Manuel Zimmer, Jesse M. Gray, Navin Pokala, Andy J. Chang, David S. Karow, Michael A. Marletta, Martin L. Hudson, David B. Morton, Nikos Chronis, and Cornelia I. Bargmann. Neurons detect increases and decreases in oxygen levels using distinct guanylate cyclases. *Neuron*, 61:865–879, 3 2009. ISSN 08966273. doi: 10.1016/j.neuron.2009.02.013.